Available online at www.sciencedirect.com
ScienceDirect
Coordination Chemistry Reviews 253 (2009) 723–753
COORDINATION CHEMISTRY REVIEWS
www.elsevier.com/locate/ccr

Review

Quantum chemical studies of molecules incorporating a $Cu_2O_2^{2+}$ core

Benjamin F. Gherman [a,b], Christopher J. Cramer [a,*]

[a] *Department of Chemistry and Supercomputer Institute, University of Minnesota, 207 Pleasant Street SE, Minneapolis, MN 55455-0431, USA*
[b] *Department of Chemistry, California State University, Sacramento, 6000 J Street, Sacramento, CA 95819-6057, USA*

Received 25 September 2007; accepted 20 November 2007
Available online 11 January 2008

Contents

Abstract

The utility of various computational models for characterizing the structure, energetics, reactivity, and spectroscopy of bare and supported $Cu_2O_2^{2+}$ cores is reviewed.

Keywords: Oxytyrosinase; Oxyhemocyanin; C–H bond activation; Aromatic hydroxylation; μ-η^2:η^2-Peroxo dicopper; Bis(μ-oxo) dicopper; Non-dynamical electron correlation; Dynamical electron correlation; Density functional theory

1. Biological systems containing $Cu_2O_2^{2+}$ cores

Chemical systems containing $Cu_2O_2^{2+}$ cores, which have been noted for the important roles they play in environmental

* Corresponding author. Tel.: +1 612 624 0859; fax: +1 612 626 2006.
E-mail address: cramer@chem.umn.edu (C.J. Cramer).

0010-8545/$ – see front matter © 2008 Elsevier B.V. All rights reserved.
doi:10.1016/j.ccr.2007.11.018

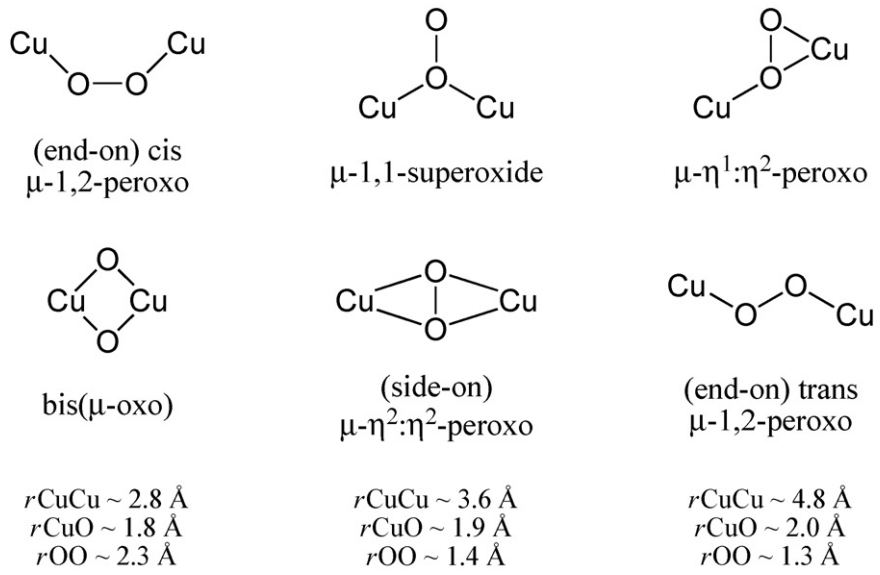

Fig. 1. Various possible coordination modes of O_2 to two copper atoms. Typical metrics for key bond distances in the core are listed for the most common three motifs, which are shown at the bottom.

chemistry [1], medicinal chemistry [2], and industrial applications [3,4], have been of particular interest because of their importance in biochemistry [5–12]. These cores form the functional center of proteins and enzymes that transport or activate, respectively, molecular oxygen (dioxygen) upon complexation of O_2 to the two copper atoms. In the enzymatic cases, reactions involving adjustments of formal oxidation states of O or O_2 fragments are facilitated by conversions between different Cu atom oxidation states that are well tuned in a redox sense to the chemistry in question.

Due to the considerable variety of ways in which two copper(I) atoms can bind molecular oxygen, a range of isomers for the $Cu_2O_2^{2+}$ core have been observed and/or proposed in different biological and biomimetic systems (Fig. 1) [12,13]. Three of these motifs – bis(μ-oxo), μ-η^2:η^2-peroxo, and *trans* μ-1,2-peroxo – have proven to be dominant, although examples of the other three in Fig. 1 have been identified or inferred. In the bis(μ-oxo) isomer, the O–O bond is broken and the copper ions are in a formal +3 oxidation state coordinated by two O^{2-} ligands. The μ-η^2:η^2-peroxo and μ-1,2-peroxo isomers, by contrast, each feature a peroxide dianion bound to two Cu(II) ions. The different isomers often exist in equilibrium with one another, with small activation energies for their interconversion [13–18].

Three type 3 copper proteins – hemocyanin, tyrosinase, and catechol oxidase – utilize $Cu_2O_2^{2+}$ cores in order to execute their respective biochemical functions. Hemocyanin, found mainly in mollusks and arthropods, functions as an oxygen transport and storage protein, to which dioxygen is reversibly bound as peroxide [19–29]. Crystal structures of the oxy form (oxyHc) demonstrate the presence of a slightly butterflied μ-η^2:η^2-peroxo $Cu_2O_2^{2+}$ core (Fig. 2a) [30–32]. Of the three histidine residues coordinated to each copper, one is located in a Jahn–Teller distorted axial position, resulting in weaker coordination to the metal center compared to the other two histidines. The bond distances within the μ-η^2:η^2-peroxo $Cu_2O_2^{2+}$ core are stereotypical for the motif (cf. Fig. 1). Oxyhemocyanin is EPR silent and exists as an antiferromagnetically coupled singlet [28,33–35].

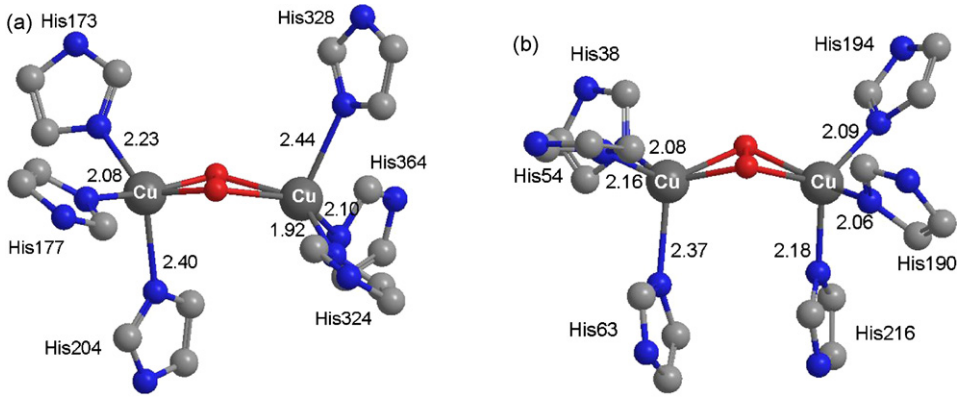

Fig. 2. Active sites from the crystal structures of (a) oxyhemocyanin [32] and (b) oxytyrosinase [43]. Distances are shown in Å. (a) Cu–O distances range from 1.72 Å to 2.18 Å, O–O distance 1.41 Å, and Cu–Cu distance 3.59 Å. (b) Cu–O distances 2.04 Å, O–O distance 1.50 Å, and Cu–Cu distance 3.55 Å.

Tyrosinase [20,21,36–40], while having an active site very similar to hemocyanin, has a distinct biological role. Occurring in eubacteria, fungi, plants, insects, and animals (including humans) [41,42], tyrosinase catalyzes the initial step in the formation of the pigment melanin from tyrosine [44], has been implicated in playing a role in the protection of injured tissues (wound protection) [45], and has been reported to be linked to neurodegenerative diseases [46,47]. Specifically, tyrosinase carries out the oxidation of phenols to *o*-diphenols (termed the cresolase reaction; Eq. (1a))

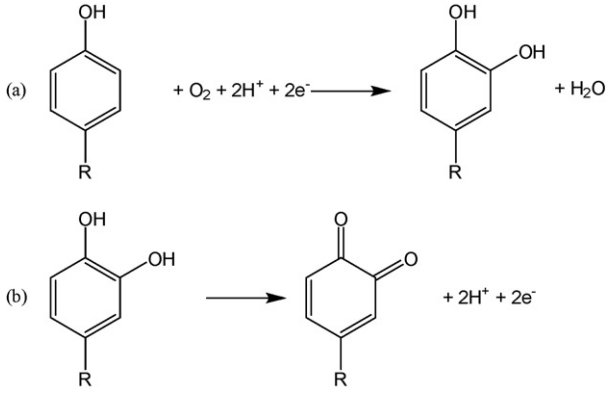

(1)

and a subsequent two-electron oxidation of the *o*-diphenol to the *o*-quinone (termed the catecholase reaction; Eq. (1b)). A crystal structure of oxytyrosinase (Fig. 2b) highlights the similarities between it and oxyhemocyanin: three histidine residues ligate each copper, one histidine per copper is in a relatively weakly bound axial position, and, most importantly, in each case there is a slightly puckered μ-η^2:η^2-peroxo $Cu_2O_2^{2+}$ core [43]. Such similarity to hemocyanin had long been suspected based upon sequence homology and spectroscopic data [21,36,48–50]. This core plays a central role in the catalytic mechanism of tyrosinase [21,39,43,51,52]. Following dioxygen activation by the coupled dicopper active site, the first key step in the cresolase and catecholase reactions involves binding of the phenol and *o*-diphenol, respectively, to the side-on μ-η^2:η^2-peroxo $Cu_2O_2^{2+}$ core (Fig. 3) [50,53]. The electronic structure of the side-on μ-η^2:η^2-peroxo $Cu_2O_2^{2+}$ core has been suggested to play an important role in its ability to catalyze the hydroxylation reaction [54–56], due to electrophilic character in the peroxide resulting from strong σ donation to the copper centers, and a weak O–O bond resulting from back-bonding from the peroxide σ^* orbital to the copper centers.

Like tyrosinase, catechol oxidase (also called *o*-diphenol oxidase or polyphenol oxidase) also catalyzes the oxidation of catechols to *o*-quinones (Eq. (2)) [21,57–59].

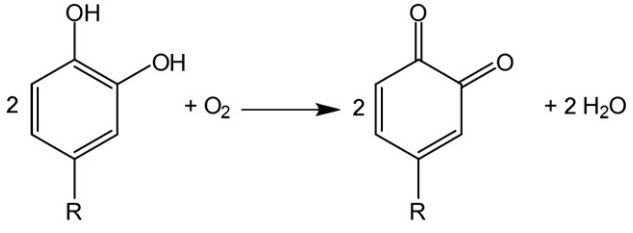

(2)

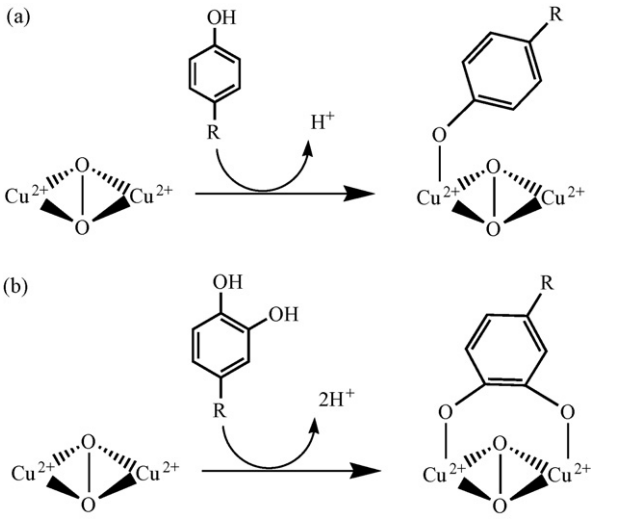

Fig. 3. Binding of (a) the phenol and (b) the *o*-diphenol to the side-on μ-η^2:η^2-peroxo $Cu_2O_2^{2+}$ core of oxytyrosinase in the cresolase and catecholase reactions, respectively [50,53].

Catechol oxidase, however, lacks the hydroxylase activity of tyrosinase that is responsible for the conversion of phenols to catechols. As with tyrosinase, catechol oxidase is involved in formation of the pigment melanin and in wound protection. The active site of catechol oxidase contains six histidines residues, three per copper, but one (His109) is covalently linked to a cysteine (Cys92) by a thioether bond [59]. The proposed catalytic mechanism invokes similar coordination of the diphenol to the $Cu_2O_2^{2+}$ core as seen in the catecholase step in tyrosinase (cf. Fig. 3b) [21,59].

A fourth enzyme, membrane-bound particulate methane monooxygenase (pMMO) [60–65], has also been suggested to contain a $Cu_2O_2^{2+}$ core. Found in methanotrophic bacteria, which use methane as their sole source of carbon and energy [66], pMMO oxidizes methane using molecular oxygen to generate methanol in the initial stages of the methane oxidation pathway leading ultimately to carbon dioxide.

$$CH_4 + NADH + H^+ + O_2 \rightarrow CH_3OH + NAD^+ + H_2O \quad (3)$$

The enzyme is remarkable for its ability to catalyze this conversion efficiently under physiological conditions. pMMO may have the potential to impact environmental concerns (e.g., global warming or bioremediation [66,67]) and the use of methane as an alternative energy source [68]. In contrast to the type 3 copper proteins, the bis(μ-oxo) motif is proposed to be responsible for hydrocarbon oxidation based on model-complex studies [14,69–75] and mixed quantum mechanical/molecular mechanical (QM/MM) calculations [76] (Fig. 4a and vide infra) based upon the crystal structure of pMMO determined by Lieberman and Rosenzweig (Fig. 4b) [65]. Specifically, the proposed mechanism involves the bis(μ-oxo) dicopper core initiating substrate oxidation by hydrogen-atom abstraction to one of the bridging oxo moieties [76].

Elucidation of the catalytic mechanisms of these metalloenzymes possessing the $Cu_2O_2^{2+}$ core has demanded accurate determination of the electronic structures and energies of the

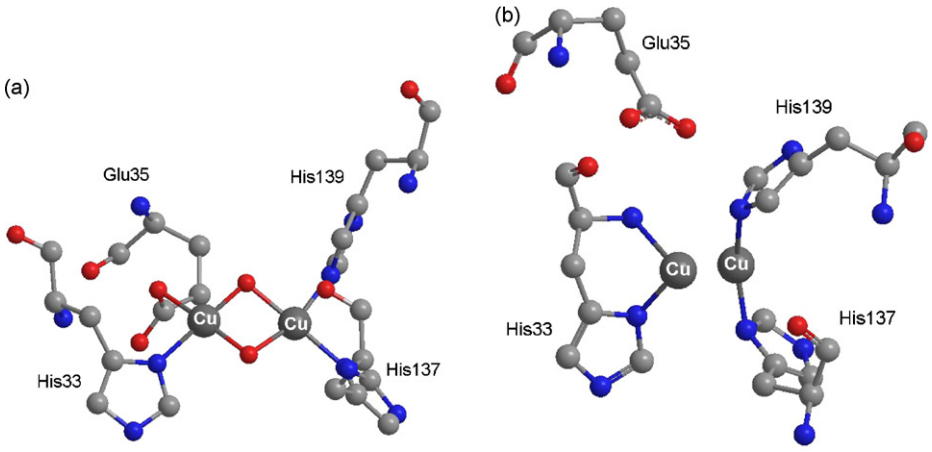

Fig. 4. (a) The bis(μ-oxo) motif in pMMO as determined by QM/MM calculations [76]. (b) The dicopper site in the crystal structure for the deoxygenated form of pMMO [65]. (a) Cu–O distances range from 1.76 Å to 1.93 Å, O–O distance 2.40 Å, and Cu–Cu distance 2.76 Å. (b) Cu–Cu distance 2.58 Å.

different core isomers. Such information would, for example, help to establish whether O–O bond scission occurs prior to or concomitant with substrate activation. It also offers the potential to advance the design of synthetic catalysts that use dioxygen as a terminal oxidant.

With such goals in mind, computational modeling of these enzymes has tended to follow one of two complementary directions. In the first approach, small models of the enzymes' active sites have been used, varying in their level of complexity with respect to representation of the biologically relevant ligands. Spanning the bare $Cu_2O_2^{2+}$ core, to the core supported by four to six ammonia ligands, to the core supported by four to six imidazole ligands, these relatively small systems (at least when compared to the active sites of the hemocyanin, tyrosinase, and catechol oxidase enzymes themselves) have enabled the application of various levels of theory ranging from self-consistent-field-Xα-scattered wave (SCF-Xα-SW) calculations, to Hartree–Fock and post-Hartree–Fock methods, to density functional theory, and to multideterminantal methods, such as complete active space and multireference configuration interaction calculations. A full discussion of this considerable body of research can be found in particular in Sections 3.2 and 3.3, and also throughout Sections 4 and 5. The main other direction of computational work has consisted of mixed QM/MM calculations on entire enzyme systems, i.e., active site plus complete protein environment, with the quantum mechanics being handled by density functional theory. Work here has been largely limited to the pMMO system and is discussed in Sections 3.2.3 and 4.2.

2. Synthetic systems containing $Cu_2O_2^{2+}$ cores

Given the similarities among the metalloenzymes hemocyanin, tyrosinase, and catechol oxidase in terms of active site structure and function, the study of biomimetic models for these systems has attracted the interest of many experimental groups [9,10,12,13,36–38,77–84]. Such smaller synthetic systems provide simpler and more readily adjusted ligand environments supporting the copper centers. Variations in properties upon modification of ligands can then offer insight into those aspects of the electronic structure of the $Cu_2O_2^{2+}$ cores that dominate structure and reactivity. While many such biomimetic ligands have been presented in the chemical literature, for the purpose of this review we will restrict our discussion to only ligand systems that have been the subject of computational investigation.

Synthetic $Cu_2O_2^{2+}$ systems may be divided into two primary groups: those in which the copper centers are each coordinated to three N donors (Fig. 5a), and those in which the copper centers are each coordinated to two N donors (Fig. 5b). In the case of triply coordinated copper(II) centers, one nitrogen is typically weakly coordinated in a pseudo-axial position as a result of Jahn–Teller distortion. If the copper center is better described as Cu(III), no Jahn–Teller effect is operative and coordination of the third nitrogen tends to be more consistent with that of the other two. Important examples of tridentate nitrogen ligands include variously substituted 1,4,7-triazacyclononanes (TACN) [3,16,71,85–93], 1,4,7-triazacyclodecane (TACD) [92,94–96], hydrotris(pyrazolyl)borate (HB(3,5-R,R′-Pz)$_3$) [97–100], and MePY2 where the amine nitrogen of a bis(2-pyridylethyl) amine unit (PY2) is substituted with a methyl group [15,93,101–103]. The MePY2 ligand has also been utilized with substituents present at the 4-position on the pyridine rings [15,93]. Other tridentate ligands include 3,3′-iminobis(*N*,*N*-dimethylpropylamine) (AN) [93,104], its methyl-substituted variant MeAN [93,104], and *N*-[2-(pyridin-2-yl)ethyl]-*N*,*N*,*N*′-trimethyl-propane-1,3-diamine (PYAN) [17,93]. Related effectively tridentate ligands are Schiff-base dinucleating ligands containing two tridentate binding sites linked by a xylyl spacer [105–108] and hexaaza *N*-hexadentate macrocyclic dinucleating ligands based on a *m*-xylyl spacer [106,109].

The observed Jahn–Teller structural distortion in the Cu(II)$_2$O$_2^{2+}$ systems supported by tridentate ligands has prompted the suggestion that bidentate nitrogen ligation of each copper center ought already to be sufficient to stabilize the $Cu_2O_2^{2+}$ cores. Bidentate ligands are attractive from a catalytic viewpoint as they should in general offer exogenous substrates increased access to the core. Bidentate ligands

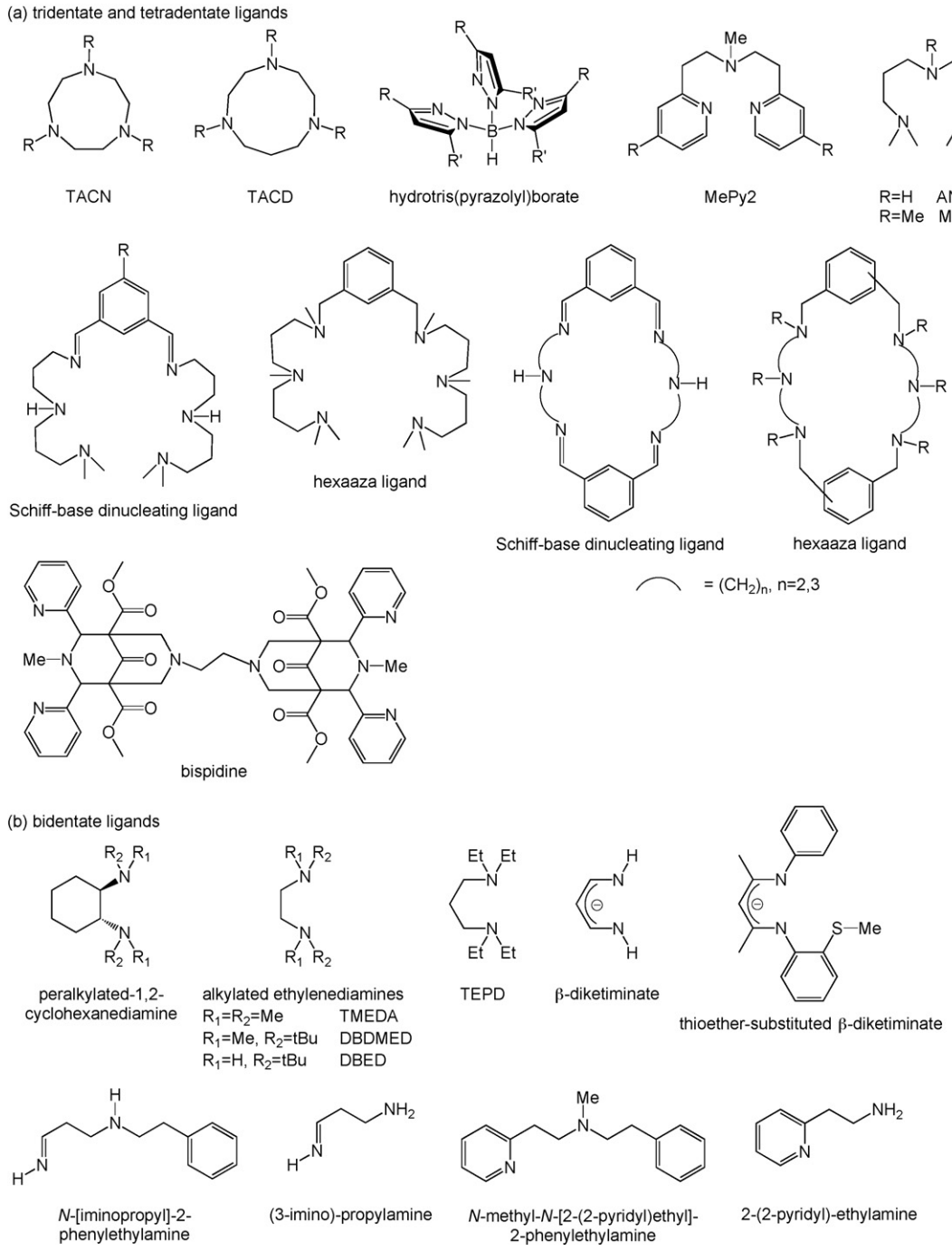

Fig. 5. Synthetic (a) tridentate and tetradentate ligand systems and (b) bidentate ligand systems used to support $Cu_2O_2^{2+}$ cores. All ligands systems shown here have been the subject of computational study in addition to experimental work.

developed to explore these possibilities consist of peralkylated-1,2-cyclohexanediamines [99,110]; alkylated ethylenediamines including *N*,*N*,*N*′,*N*′-tetramethylethylenediamine (TMEDA) [3], *N*,*N*′-di-*tert*-butyl-*N*,*N*′-dimethylethylenediamine (DBDMED) [96], and *N*,*N*′-di-*tert*-butyl-ethylenediamine (DBED) [18,96,111,112]; and *N*,*N*,*N*′,*N*′-tetraethylpropane-1,3-diamine (TEPD) [113]. The anionic β-diketiminate ligand [114–116] and its thioether-substituted variant [117] have also been shown to stabilize $Cu_2O_2^{2+}$ cores. The ligands *N*-[iminopropyl]-2-phenylethylamine, (3-imino)-propylamine, *N*-methyl-*N*-[2-(2-pyridyl)ethyl]-2-phenylethylamine, and 2-(2-pyridyl)-ethylamine have been studied as well [74,118].

Lying outside of this dichotomy of ligands is the tetradentate ligand bispidine (Fig. 5a), a dinucleating derivative of 3,7-diazabicyclo[3.3.1]nonane with a bis-tertiary-amine-bispyridyl donor set [119–123], use of which leads to a *trans* μ-1,2-peroxo intermediate according to molecular mechanics calculations [123]. Another member of this category is a system composed of two different ligands which supports dual tri-coordinate copper(I) centers, the bis(μ-pyradizine)bis(1-

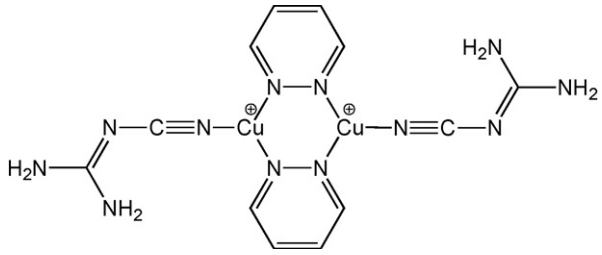

Fig. 6. Structure of the $[Cu_2(\mu\text{-pydz})_2(cnge)_2]^{2+}$ dicopper(I) cation.

cyanoguanidine) dicopper(I) cation ($[Cu_2(\mu\text{-pydz})_2(cnge)_2]^{2+}$) (Fig. 6) [124,125], which is capable of forming adducts with molecular oxygen.

An alternative way to divide these ligands into two classes is to note that some support mononuclear complexes that self-assemble (dimerize) upon reaction with dioxygen while others are dinucleating ligands that encourage O_2 binding by spatial preorganization of the two metal ions. Members of the latter class, which include the Schiff-base [105–108] and hexaaza ligands [106,109], as well as bispidine [119–123], offer the possibility of enforcing particular ranges of metal–metal distances.

A final classification scheme might involve consideration of which ligands favor end-on μ-1,2-peroxo isomers (*cis* or *trans*) of the $Cu_2O_2^{2+}$ core, which side-on μ-η^2:η^2-peroxo isomers, and which bis(μ-oxo) isomers. Of course, in particular instances an equilibrium between two or more of these motifs might be observable under experimental conditions. In general, tetradentate ligands have been found to favor end-on peroxo products upon oxygenation, while bidentate ligands have generally been found to favor the bis(μ-oxo) isomer (owing in part to their ability to accommodate well the square planar coordination geometry favored by Cu(III) centers). The situation with tridentate ligands is less clear, however, as they preferentially stabilize one or another of the isomers depending on the precise steric and electronic characteristics of the ligands themselves. Any attempt to employ a classification scheme based on oxygenated product preferences proves complicated insofar as equilibria between isomers are known and these equilibria can be particularly sensitive to solvent, temperature, and counter ions [10,16,113].

Of course, it is precisely this intriguing richness associated with the chemistry of synthetic $Cu_2O_2^{2+}$ systems that has spawned great theoretical interest and led to efforts to understand trends – or apparent lacks of trends – in terms of the electronic structures and, particularly, relative energetics of the various $Cu_2O_2^{2+}$ isomers. Computational tools have similarly been brought to bear in order to predict and explain the relative reactivities of various isomers with hydrocarbon substrates. The relatively large size of the synthetic systems (compared, for example, to active site models constructed from ammonia ligands) has led to the widespread use of the relatively efficient density functional level of theory [126,127] for the modeling of these complexes, occasionally supplemented by use of the integrated molecular orbital molecular mechanics (IMOMM) methodology [128] to handle the more sterically bulky of the synthetic ligands. A complete analysis of these computational investigations can be found in Section 3.4; we proceed next to address the particular challenges associated with the computational modeling of supported $Cu_2O_2^{2+}$ cores.

3. Quantum chemical characterization of isomerization equilibria

Amongst the various properties of molecules containing $Cu_2O_2^{2+}$ cores, one that is of key interest is the energetic profile associated with isomerization between the *trans* end-on peroxo (μ-1,2; henceforth when we use "end-on peroxo" we will imply *trans* unless *cis* is specified), side-on peroxo (μ-η^2:η^2), and bis(μ-oxo) forms. To the extent that such isomerizations may be facile and the relative reactivities of these various isomers may be different [10], their relative energies and the facility with which they may interconvert are attractive targets for computation.

3.1. Qualitative considerations

As with any computational modeling effort, some compromise must typically be made in the manner in which the experimental system is represented in order to render the calculation tractable. In practice, the ligands supporting experimentally characterized $Cu_2O_2^{2+}$ cores have tended to be of moderate to large size, e.g., three imidazole ligands per copper in the active site of oxyhemocyanin, or *N*,*N*′,*N*″-trialkyltriazacyclononane or *N*,*N*′-diaryldiketiminate ligands in synthetic model systems. Given the non-trivial size of such ligands, modeling studies have tended to focus either on smaller ligands (e.g., ammonia) where fairly complete levels of electronic structure theory with large one-electron basis sets can be applied, or the full or near-full ligand systems have been employed but the basis sets have been adjusted to be more flexible in the region of the core than in "unimportant" regions of the ligands. Thus, for example, the minimal STO-3G basis set might be used for H atoms substituting distant positions of a large organic ligand. Demonstrating convergence with respect to the size of the one-electron basis set can be difficult when the ligand is represented in full. However, experience with basis set convergence developed with small model ligands may be transferable to more realistic ligands where the issue is more difficult to assess.

An additional basis set issue involves the choice of using an all-electron basis set or an effective core potential for copper. As the latter choice not only reduces the size of the electronic structure problem, but also permits relativistic effects to be included directly into the core potential, it has tended to be the more typical approach. Popular pseudopotentials for Cu include the small (10-electron) core Stuttgart–Dresden basis set of Dolg et al. [129,130] and the small (10-electron) [131] or large (18-electron) core Hay–Wadt basis sets [132] (sometimes also called LAV and LACV, respectively, in various electronic structure programs). In the case of the Hay–Wadt basis sets, relativistic effects are *not* included in the pseudopotentials for first-row transition metal atoms like Cu.

A final point bearing on comparisons of computed and experimental quantities for $Cu_2O_2^{2+}$ cores is the surrounding medium.

All experimental equilibrium data have been measured in solution; moreover, unless the supporting ligands are anionic, the solutions necessarily include counterions to balance the 2+ charge of the core. It is not obvious how best to include these effects in the computational models. Insofar as the most commonly used experimental solvents have relatively low dielectric constants (e.g., dichloromethane or tetrahydrofuran) one may expect ion pairs to be prevalent. On the other hand, the typical counterions are usually non-nucleophilic (e.g., perchlorate or hexafluoroantimonate) so direct coordination to copper may not be strong. Unfortunately, including them in a gas-phase calculation is likely to strongly overemphasize their importance (because they will be substantially more nucleophilic in the absence of solvation) in addition to substantially increasing the expense of the computation.

More general solvation effects can be included using continuum dielectric models [133]. When the models are charged, the dominant portion of the solvation free energy is associated with the Born term, which is inversely proportional to the radial size of the system, so that solvation tends to favor the more compact bis(μ-oxo) form [93,134] over the more extended peroxo forms. However, an implicit solvation model ignores the possible influence of solvents acting as actual ligands at open coordination sites. Depending on the nature of the supporting ligands, such coordination may be unlikely, but specific solvation has been demonstrated to play a role in the kinetics of oxygen activation by monocopper species [135], so it is not out of the question that it may be important in $Cu_2O_2^{2+}$ cores as well, although the point remains to be explored computationally.

3.1.1. Limiting oxidation numbers/resonance structures

In order to appreciate the different challenges that particular supported $Cu_2O_2^{2+}$ isomers may pose to various levels of electronic structure theory, it is instructive to consider the limiting redox states that might be assigned to them in a classical inorganic ion sense. Thus, the bis(μ-oxo) form would be represented by two Cu(III) ions coordinated to O^{2-} oxide anions, while the end-on and side-on peroxide isomers would be classically represented as incorporating Cu(II) ions together with the O_2^{2-} fragment. The distinction is potentially critical because of the different nature of Cu(II) and Cu(III), the former being d^9, and thus intrinsically open-shell at the metal, while the latter is d^8, and given a strong ligand field would be expected to be closed-shell at the atom. Essentially all electronic-structure theories are well suited to the description of closed-shell singlet wave functions. However, the limiting case of two d^9 copper atoms is much more challenging. If the two spins on the two metals were to couple ferromagnetically, i.e., to generate a triplet spin state, such a state would be well represented by a single Slater determinant [126] and continue to be amenable to standard levels of theory. However, when the coupling is antiferromagnetic, as has been found in all experimentally characterized peroxides, the molecules are formally singlet biradicals and the representation of such biradicals cannot be accomplished with a single Slater determinant [126], leading to potentially severe complications for single-reference theoretical models like standard Hartree–Fock, post-Hartree–Fock, and Kohn–Sham density functional theory approaches. The preference for the singlet state ($-2J$ in the Heisenberg formulation of the spin states) in the side-on peroxo isomer coordinated by six ammonia ligands has been estimated by various theoretical approaches to be 1200–5000 cm^{-1} [134,136,137], with substantial variation associated with different ligands. So, while the antiferromagnetic coupling is not especially weak, neither is it so strong that biradical character can be discounted.

3.1.2. Implications for different theoretical formalisms

A true singlet biradical, characterized by two electrons in two orbitals, requires two determinants for its representation in wave function theory [126]. In the case of a peroxide $Cu_2O_2^{2+}$ isomer we might write a singlet wave function for the two highest-energy electrons as

$$^1\Psi_{2D} = \frac{1}{2}[Cu_a(1)Cu_b(2) + Cu_a(2)Cu_b(1)] \begin{vmatrix} \alpha(1) & \beta(1) \\ \alpha(2) & \beta(2) \end{vmatrix} \quad (4)$$

where the electrons are indexed as 1 and 2, the copper atoms are separately identified as a and b, α and β are the usual spin functions, which appear in the determinant on the right-hand-side that represents the singlet spin function, and the superscript on Ψ indicates the wave function to be singlet and the subscript emphasizes that it is formed from two determinants. A standard restricted formalism, whether in the context of Hartree–Fock (HF) theory or Kohn–Sham density functional theory (DFT), cannot be used to represent this wave function, but is instead restricted to a single determinant (1D) that derives from spin pairing the two electrons in a single orbital, e.g.:

$$^1\Psi_{1D} = \frac{1}{\sqrt{2}}[Cu_x(1)Cu_x(2)] \begin{vmatrix} \alpha(1) & \beta(1) \\ \alpha(2) & \beta(2) \end{vmatrix} \quad (5)$$

where x is either a or b. This wave function is ionic, in the sense that both electrons are on one copper while the other has none, and as such the energy of the wave function is unrealistically high (Note, as a technical point, that DFT as a theory need not formally make reference to wave functions of any sort. However, in order to compute the electronic kinetic energy, the almost universally employed Kohn–Sham implementation of DFT *does* invoke a wave function for a system of non-interacting electrons [126], and thus it is also typically sensitive to this issue, although interpretation of the Kohn–Sham non-interacting wave function may be criticized [138].).

In order to recover the so-called non-dynamical correlation energy that is associated with the two-determinantal wave function, single-determinantal models like HF and DFT can be allowed to break *spin* symmetry, employing instead of Eq. (5) the determinant:

$$^{1|3}\Psi_{1D} = \frac{1}{\sqrt{2}} \begin{vmatrix} Cu_a(1)\alpha(1) & Cu_a(1)\beta(1) \\ Cu_b(2)\alpha(2) & Cu_b(2)\beta(2) \end{vmatrix} \quad (6)$$

While this single determinant does place one electron on each copper atom, and is properly antisymmetric, it is *not* an eigenfunction of the total spin operator S^2. Evaluation of $\langle S^2 \rangle$ returns a value of 1.0, which indicates that the wave function is instead

an equal mixture of singlet ($\langle S^2\rangle = 0$) and triplet ($\langle S^2\rangle = 2$) states, and to emphasize this the left superscript 1|3 has been added to Ψ. The determinant of Eq. (6) is potentially useful because if the Hamiltonian operator does not include spin–orbit coupling (which is to say that matrix elements of the Hamiltonian operator H between different spin states must be zero), then we may evaluate its expectation value for ${}^{1|3}\Psi_{1D}$ as

$$\begin{aligned}
&\langle {}^{1|3}\Psi_{1D}|H|{}^{1|3}\Psi_{1D}\rangle \\
&= \frac{1}{2}\langle {}^1\Psi + {}^3\Psi|H|{}^1\Psi + {}^3\Psi\rangle \\
&= \frac{1}{2}\left[\langle {}^1\Psi|H|{}^1\Psi\rangle + \langle {}^1\Psi|H|{}^3\Psi\rangle + \langle {}^3\Psi|H|{}^1\Psi\rangle + \langle {}^3\Psi|H|{}^3\Psi\rangle\right] \\
&= \frac{1}{2}({}^1E + 0 + 0 + {}^3E) = \frac{{}^1E + {}^3E}{2}
\end{aligned} \tag{7}$$

Thus, the expectation value of the broken-symmetry determinant is the average energy of the singlet and triplet states. Since the triplet state energy can be computed independently from the high-spin single determinant

$${}^3\Psi_{1D} = \frac{1}{\sqrt{2}}[\alpha(1)\alpha(2)]\begin{vmatrix} Cu_a(1) & Cu_b(1) \\ Cu_a(2) & Cu_b(2) \end{vmatrix} \tag{8}$$

one may then determine the singlet state energy as the only unknown in Eq. (7).

The approach outlined above was originally employed by Ziegler et al. [139] and Noodleman and Norman [140] to compute the energies of spin states in primarily inorganic systems that would be otherwise inaccessible to single-determinantal DFT. In cases where the spatial orbitals in the broken symmetry wave function have non-zero overlap, $\langle S^2\rangle$ can take on values other than precisely 1, in which case an analogous analysis indicates that the singlet energy may be computed conveniently from [141]:

$${}^1E = \frac{2^{BS}E - \langle S^2\rangle_{BS}{}^3E}{2 - \langle S^2\rangle_{BS}} \tag{9}$$

where $\langle S^2\rangle_{BS}$ refers to the value computed for the broken-symmetry wave function having energy ${}^{BS}E$. This approach has been exploited for the determination of singlet-state energies in various open-shell organic and inorganic systems exhibiting restricted to unrestricted singlet instabilities [142–156], including the $Cu_2O_2{}^{2+}$ cores that are the primary subject of this review [93,134,137,157,158]. We note that another recently developed approach, spin-flip DFT [159], permits computation of the energies of multideterminantal states by an alternative approach, generating them as excited states from a typically high-spin single-determinantal reference. Preliminary results are encouraging for monocopper–O_2 cases [160], for instance, and it will be interesting to continue to evaluate this model moving forward. Davidson and Clark have recently analyzed different methods used in conjunction with broken-symmetry wave functions [161], and interested readers are referred there for further discussion.

As a technical aside, there is some confusion in the literature with respect to KS DFT applied to such a singlet biradical as that represented by the Cu(II)/Cu(II) formulation of a $Cu_2O_2{}^{2+}$ core. One occasionally sees it written that a restricted singlet DFT KS wave function must be "wrong" if that wave function is *stable* to symmetry breaking, the rationale being that there *must* be an α electron on one copper and a β electron on the other, and that such an orbital localization can only happen by symmetry breaking. This is fundamentally incorrect, however, because a singlet state has zero spin density at every position in space. To the extent that the Cu atoms are d^9, there should be 9 electrons worth of *paired* spin density associated with each Cu atom, but there is *nowhere* a localized region having any excess spin. Thus, in a formal sense, a restricted DFT singlet solution is more appealing than a broken-symmetry one; however, that is not to say that there is any guarantee that the stable wave function in question will provide a good energy—that issue must be judged independently [148,162]. The point we wish to emphasize here is that spin-symmetry breaking, as a phenomenon, is neither "right" nor "wrong" for any particular calculation—it simply reflects a tendency to add correlation energy that may be insufficiently present in some particular restricted single-determinantal DFT calculation. It should be kept in mind that formal density functional theory (as opposed to its Kohn–Sham implementation) is entirely compatible with an orbital-free formulation. Thus, the exact functional would return the exact energy for the exact singlet density, which would have no localized spin at any position. It remains an open question in electronic structure theory whether any arbitrary density can indeed be generated by a single Slater determinant, and moreover most modern functionals developed for Kohn–Sham calculations are not exact, but are instead approximate. Thus, it is essentially impossible to predict the degree to which such functionals may accurately represent biradical character in restricted self-consistent-field solutions except, of course, by comparison to experiment or other well-converged calculations.

The above discussion is primarily relevant for DFT. In wave function theory (WFT), on the other hand, correlation energy, whether non-dynamical or dynamical, can be recovered via post-HF procedures even if a single-determinant reference is expected to be itself of poor quality. Of course, WFT models are by no means restricted to single determinants; multiconfigurational self-consistent field (MCSCF) theory [163] handles multiple determinants by construction, and the complete active space (CAS) variant [164] is quite robust for the comparison of different spin states, particularly after accounting for additional dynamical correlation effects via a multireference second-order perturbation theory like CASPT2 [165,166]. While formally appealing, however, the multireference models have their own practical limitations associated with the size of the active space, that is, the number of molecular orbitals that need to be permitted to have occupation numbers other than 0 or 2. In practice, modern theory is limited to a consideration of roughly 14 electrons in 14 orbitals. An ideal prescription for a $Cu_2O_2{}^{2+}$ core, however, might arguably include all of the valence orbitals of the 4 atoms: 4s and 3d orbitals on Cu (assuming that the 3p are energetically not especially important) and 2s and 2p on O. This prescription alone results in 20 orbitals, and since the Cu d shell is nearly full, one really should account for the so-called "double-shell effect"

and include a set of 4d orbitals that can be used to correlate the filled 3d orbitals. As such an active space of 28 electrons in 30 orbitals is vastly in excess of anything accessible to modern CAS implementations, one is forced to try to truncate the space in a chemically sensible fashion as discussed in more detail below. Unfortunately, this process is not guaranteed to be successful.

Alternatively, one can continue with a single reference and account for electron correlation via post-HF approaches, e.g., perturbation theory, configuration interaction (CI), or coupled-cluster (CC) theory. Perturbation theory starting from a poor reference configuration, however, typically leads to very poor convergence behavior with respect to consideration of increasingly higher-order terms in the perturbation expansion. CI is a more expensive approach that suffers from its failure to be size extensive. CC theory, on the other hand, is generally more robust than perturbation theory and is size extensive. Because the computational resources required for CC theory scale roughly with the seventh power of the size of the molecular system, its application tends to be limited to smaller models. In its completely renormalized variant (CR-CC [167]) it is especially suited for the treatment of biradicaloid systems [168,169].

3.2. Single-reference theories applied to model systems

This section, as well as Section 3.3, is primarily concerned with comparisons of different computational models one to another with the goal of establishing validated theoretical protocols and understanding computational limitations

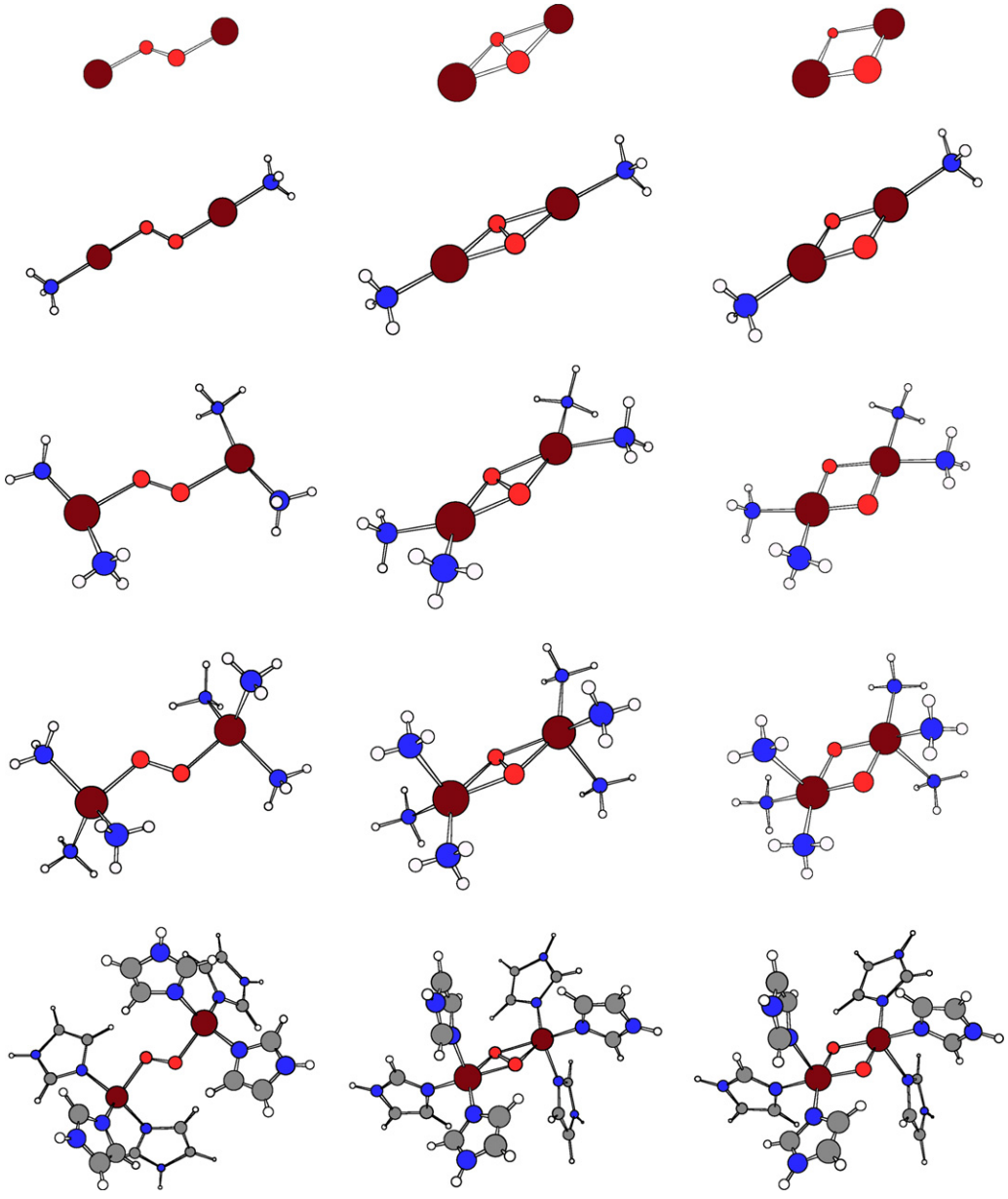

Fig. 7. Ball-and-stick representations of end-on peroxo (left), side-on peroxo (center), and bis(μ-oxo) (right) isomers of $[(NH_3)_nCu]_2O_2^{2+}$ ($n=0$–3) and $[(imid)_3Cu]_2O_2^{2+}$ whose relative energies are compared at various theoretical levels below. Geometries are taken from Refs. [157,158]; Cu atoms, brown; O, red; N, blue; C, gray; H, white. (For interpretation of the references to color in this figure legend, the reader is referred to the web version of the article.)

introduced by details of electronic structure in key isomers. In order for the most sophisticated levels of electronic structure theory to be practical, many researchers have chosen to examine model systems containing simplified ligands, particularly ammonia (NH_3). A substantial amount of the discussion below will therefore focus on systems $[(NH_3)_nCu]_2O_2^{2+}$ ($n = 0$–3; Fig. 7).

Of course, an alternative to comparing theories one to another in order to establish a benchmark is instead to compare theories to quantitative experimental data where available. Some such comparisons are indeed noted in the discussion of the model systems in this section and Section 3.3, but for the most part such an analysis is deferred instead to Section 3.4.

3.2.1. Hartree–Fock

As a small bit of history to enliven this review, following a 1995 squash match between one of the authors (CJC) and his experimental colleague, Bill Tolman, discussion turned to a potential new dicopper–dioxo species that had been synthesized in the Tolman labs, but for which all efforts at crystallization had failed to succeed. Based on unique UV and resonance Raman spectral characteristics, Tolman suspected the core of $[(Bn_3TACN)Cu]_2O_2^{2+}$ to have a bis(μ-oxo) geometry, a motif not previously observed in dicopper–dioxo chemistry. Tolman was curious whether theory might offer a "quick and dirty" confirmation of whether such a structure might be plausible. Cramer suggested that he knew of no level of theory quicker nor dirtier than HF/STO-3G, particularly if the complex TACN ligand were to be replaced by three ammonias, and suggested that if Tolman could wait a few hours, a prediction might be forthcoming. With the convenient C_{2h} symmetry of the model, it took very little time for the calculation to finish, and indeed a bis(μ-oxo) structure proved to have all real frequencies and it was offered to Tolman (and his collaborator Larry Que) with the apologetic caveat that this level of theory was somewhere between rudimentary and embarrassing. To Cramer's surprise, 1 week later a crystal structure was finally obtained and his colleagues considered the experimental metrics to be in sufficiently good agreement with the theoretical prediction to merit felicitations. Owing no doubt to fortuitous cancellation of errors, and to the closed-shell nature of the Cu(III) motif, the computed HF/STO-3G vibrational frequency and its ^{18}O isotope shift for a key core breathing frequency (see Section 5.1) were also in excellent agreement with experiment, and the theoretical results were included in initial papers reporting the characterization of this new structural motif and rationalizing various spectral features, including those associated with ligand dynamical behavior (essentially rotation of one metal's ligand framework about the Cu–Cu axis to generate staggered and eclipsed structures) [71,86].

While the HF/STO-3G calculations of Cramer et al. [134] were obviously too crude to be of any utility with respect to energetics, they did offer molecular orbitals (MOs) suitable for a qualitative description of the mechanism of isomerization between the side-on peroxo and bis(μ-oxo) minima for $[(NH_3)_3Cu]_2O_2^{2+}$ (Fig. 8). At this level, the highest occupied MO (HOMO) for both isomers, denoted $12a_u$ in the C_{2h} point group, is predicted to be the in-phase combination of the Cu d_{xy} orbitals (taking the z-axis as perpendicular to the plane of the $Cu_2O_2^{2+}$ core), as might be expected given the coordination of the ligands. The next higher orbital in the a_u irreducible representation, a virtual orbital, is the out-of-phase combination of oxygen p_y orbitals that corresponds to the σ^*_{OO} antibonding orbital in the side-on peroxo geometry. Movement along the coordinate that reduces the Cu–Cu distance thus smoothly transfers electronic charge from the Cu d orbitals to σ^*_{OO}, thereby formally oxidizing the Cu(II) atoms to Cu(III) and breaking the O–O bond while reducing the peroxide O^- atoms to O^{2-} oxides. The near degeneracy of the $12a_u$ and $13a_u$ orbitals in the bis(μ-oxo) isomer leads to substantial stabilization via dynamical electron correlation, so that the reaction coordinate resembles in some sense an organic electrocyclic reaction. This analysis was later corroborated by Liu et al. [170] and Henson et al. [171] using Kohn–Sham orbitals (vide infra).

With respect to energetics, the inadequacy of the HF level has always been recognized, so relatively little discussion of HF energetics has ever appeared. However, insofar as HF wave functions are required as a first step in post-HF treatments, the data are available in the literature. Cramer et al. [157,158] report, for instance, that at the RHF level with basis sets of essentially triple-ζ quality, the end-on peroxo, side-on peroxo, and bis(μ-oxo) isomers of $[(NH_3)_3Cu]_2O_2^{2+}$ have relative energies of 0.0, 0.0, and -0.8 kcal mol^{-1}, respectively (using geometries optimized at the B3LYP level [172–175] with the 6-31G(d) basis set [176] on light atoms and the Stuttgart pseudopotential basis set for Cu [129,130]). Post-HF corrections to these energies thus dictate the relative energetics, since the RHF level predicts all three isomers to be essentially degenerate in energy.

3.2.2. Post-Hartree–Fock

The simplest post-HF treatment is second-order perturbation theory [126]. For the end-on peroxo, side-on peroxo, and bis(μ-oxo) isomers of $[(NH_3)_3Cu]_2O_2^{2+}$ just noted above, Cramer et al. [157,158] predicted the relative MP2/TZP energies to be 61.6, 0.0, and 69.0 kcal mol^{-1}. Thus, at the MP2 level, differential correlation energies in excess of 60 kcal mol^{-1} are predicted, with the side-on peroxo isomer enjoying substantially larger stabilization than the other two isomers. However, the enormous size of the differential perturbation corrections and the large mag-

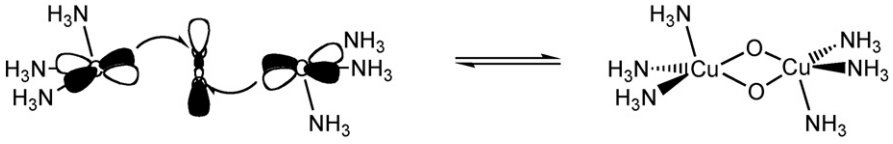

Fig. 8. Orbital interaction that converts side-on peroxo to bis(μ-oxo) in $[(NH_3)_3Cu]_2O_2^{2+}$.

nitudes of the isomeric relative energies, which would seem to be inconsistent with known equilibria in experimental systems (although, of course, such systems are not supported by ammonia ligands), suggest that there is little reason to believe the perturbation theory results to be anywhere near converged. And, given the instability of the RHF wave functions with respect to multideterminantal character, it is not clear that one *should* expect perturbation theory to be ultimately convergent.

Turning to a more complete level of post-HF theory, Nikolov et al. [177] reported small-basis set QCISD(T) energies for different isomers of the bare $Cu_2O_2^{2+}$ core, however the methodologies employed by these authors are rather poorly described (e.g., CAS calculations were performed without specification of the numbers of active electrons or orbitals) so it is difficult to make comparisons to other work. In addition, somewhat bizarre results are described, e.g., reporting that the only stable RHF geometry of side-on peroxo $[(NH_3)_3Cu]_2O_2^{2+}$ was found to have an O–O distance of 1.24 Å and a Cu–Cu distance of 4.9 Å (cf. data in Fig. 1 above), so data from this paper are not further discussed.

The most robust post-HF treatment starting from single-determinantal RHF references that has been applied to $[(NH_3)_nCu]_2O_2^{2+}$ ($n = 0$–3) equilibria is the rigorously size-extensive CR-CC(2,3),D approach of Piecuch and co-workers, which is based on a biorthogonal formulation of the method of moments of coupled cluster (CC) equations (a formalism used to design all completely renormalized (CR) CC methods [167,178–180]) employing the left eigenstates of the similarity-transformed Hamiltonian of CC theory [181–183]. Equilibrium energetics results at the CR-CC(2,3),D level, including triple and, in small cases, quadruple excitations, for zero to three ammonia ligands on each copper are presented graphically in Fig. 9, where intermediate points between the nominal equilibrium structures represent geometries generated by linear transit between them [157,158]. Such transit paths would be expected to overestimate isomerization barriers, and by quite significant margins in the case of end-on to side-on peroxo isomerization

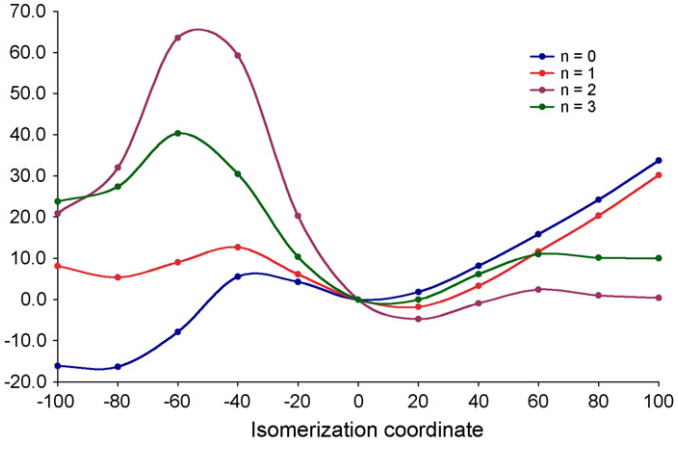

Fig. 9. Relative CR-CC(2,3),D energetics of $[(NH_3)_nCu]_2O_2^{2+}$ ($n = 0$–3) proceeding from end-on peroxo to side-on peroxo to bis(μ-oxo), these isomers being associated with values of −100, 0, and 100, respectively, on the isomerization coordinate. The side-on peroxo isomer is taken always to be the relative zero of energy.

[158], but connecting the isomers is useful for ensuring consistent choices of reference determinants and for comparison to other levels of theory (vide infra).

Cramer et al. have argued that the CR-CC(2,3),D level should be treated as providing accurate benchmark values for purposes of evaluating other levels of electronic structure theory for the computation of isomerization energetics [157,158]. This assertion was based on several arguments. First, the CR-CC(2,3),D values were observed to be reasonably well converged with respect to inclusion of high-order correlations and accounting for size-extensivity. Second, studies of *organic* biradicals have demonstrated the CR-CC model to provide accurate results compared to experiment [168,184,185]. Finally, the various curves in Fig. 9 are qualitatively sensible and, as discussed below, in quantitative agreement with other levels of theory that might also be expected to be accurate.

With respect to qualitative features in Fig. 9, if one examines the variation in the predicted end-on versus side-on energetics as a function of the number of ligands, one expects the significant Coulombic repulsion between the two copper cations to favor end-on over side-on, and side-on over bis(μ-oxo), but that effect should be reduced as ammonia ligands are added, since charge transfer can mitigate the repulsion. As electrostatics becomes less dominant, the increased covalent interactions between the copper atoms and side-on oxygen compared to end-on oxygen become manifest, so that the former isomer moves to increasingly lower energy relative to the latter (the effect has roughly saturated by the third ammonia ligand). Similarly, the bis(μ-oxo) isomer drops in energy relative to the side-on peroxo with increasing ligation, with the largest effect occurring at the point of having 2 ammonia groups supporting each copper atom, and then a modest decrease in stability of the bis(μ-oxo) relative to the side-on peroxo as a third ammonia is added to each copper. This behavior is entirely consistent with the known relative stabilities of these compounds when comparing bidentate supporting ligands to tridentate ones [12]. We will thus continue to evaluate other levels of theory against CR-CC(2,3),D below.

3.2.3. Density functional theory

Continuing to focus on the $[(NH_3)_nCu]_2O_2^{2+}$ ($n = 0$–3) family, Cramer et al. [157,158] compared the performance of a number of different functionals to CR-CC(2,3),D for the end-on peroxo/side-on peroxo/bis(μ-oxo) isomerization energetics. Fig. 10 shows results for $[(NH_3)_2Cu]_2O_2^{2+}$ using the BLYP and B3LYP functionals, the latter of which is a hybrid functional while the former is "pure", which is to say that B3LYP includes exact HF exchange in the functional definition while BLYP does not. CAS and CASPT2 results are also shown, but discussion related to these levels is deferred to Section 3.3.

The BLYP and B3LYP results in Fig. 10 are representative of pure and hybrid functional results reported by Cramer et al. [157,158]. In general, the hybrid functionals (including also *m*PW1PW91 [186] and TPSSh [187], but B3LYP in particular), do fairly well in comparison to CR-CC(2,3),D when predicting the end-on peroxo/side-on peroxo isomerization. The pure functionals (including *m*PWPW91 [186] and TPSS [187] in addition to BLYP), on the other hand, significantly overestimate

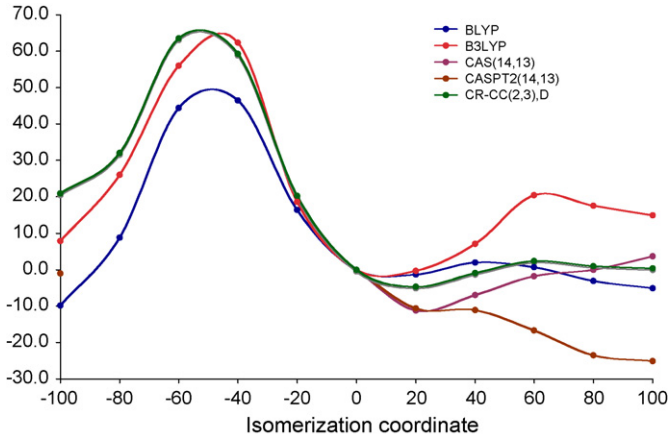

Fig. 10. Relative energetics of $[(NH_3)_2Cu]_2O_2^{2+}$ at 5 levels of theory proceeding from end-on peroxo to side-on peroxo to bis(μ-oxo), these isomers being associated with values of −100, 0, and 100, respectively, on the isomerization coordinate. The side-on peroxo isomer is taken always to be the relative zero of energy.

the stability of the end-on peroxo isomer relative to the side-on. The situation is reversed, however, for the side-on peroxo/bis(μ-oxo) isomerization. In that case, all of the pure functionals do quite well compared to CR-CC(2,3),D, but the hybrid functionals underestimate the stability of the bis(μ-oxo) isomer, with the degree of underestimation being proportional to the amount of exact HF exchange in the functional: an error of 5–10 kcal mol^{-1} for every 10% HF exchange included.

This behavior is observed in other members of the $[(NH_3)_nCu]_2O_2^{2+}$ (n = 0–3) family as well. The case of $[(NH_3)_3Cu]_2O_2^{2+}$ is illustrated in Fig. 11, which also includes results for the side-on peroxo/bis(μ-oxo) isomerization computed by Rode and Werner [188] at the multireference CI level (vide infra). The good agreement between CR-CC(2,3),D, MRCI, and BLYP for the energy difference between the canonical side-on peroxo and bis(μ-oxo) structures adds confidence to the results.

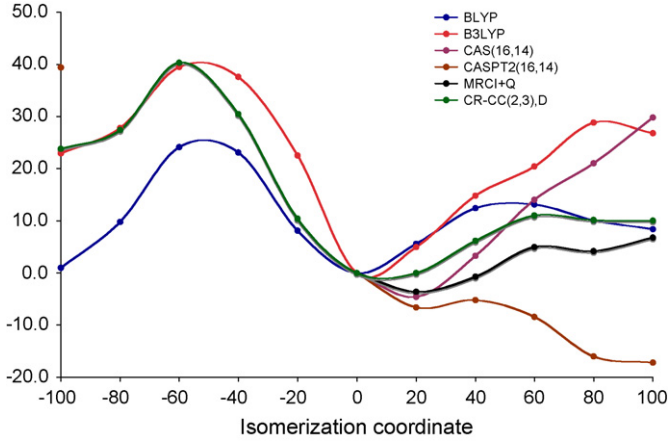

Fig. 11. Relative energetics of $[(NH_3)_3Cu]_2O_2^{2+}$ at 6 levels of theory proceeding from end-on peroxo to side-on peroxo to bis(μ-oxo), these isomers being associated with values of −100, 0, and 100, respectively, on the isomerization coordinate. The side-on peroxo isomer is taken always to be the relative zero of energy.

The apparent disparity in behavior between hybrid and pure functionals is probably more clearly understood if one temporarily adopts the energy of the bis(μ-oxo) as the relative zero of energy. In that case, one would say that the hybrid functionals overstabilize the end-on and side-on peroxo isomers relative to the bis(μ-oxo), and that the overstabilization increases with increased HF character in the functional, and the pure functionals overstabilize only the end-on peroxo isomers. Importantly, this precisely reflects the degree to which the Kohn–Sham wave functions for the peroxo species are unstable to symmetry breaking. With pure functionals, the side-on peroxo isomers often show stable restricted KS wave functions, or at most rather weak instabilities based on computed $\langle S^2 \rangle$ values, but with hybrid functionals there is much more significant mixing of singlet and triplet wave functions (a similar sensitivity to HF exchange in the functional has been observed in $Fe_2O_2^{4+}$ cores [189]). With both kinds of functionals the end-on peroxo isomers are computed to have essentially 50:50 singlet:triplet KS wave functions. This is critical because all functionals predict stable restricted KS wave functions for the bis(μ-oxo) isomers (which, being formally Cu(III) species have negligible biradical character). Thus, symmetry breaking, even with spin purification, appears to overstabilize the peroxo isomers when it occurs, and the problem grows worse with increased HF exchange in the functional because the triplet state, with its two unpaired electrons, benefits more from exact exchange than the singlet. From a practical standpoint, this is an unfortunate situation, since no single functional seems well suited to considering reactive schemes that might encompass all three kinds of bonding.

Benchmarking DFT is an important undertaking because this level of theory is really the only one practical for systems that more closely resemble those studied experimentally, e.g., $[(imid)_3Cu]_2O_2^{2+}$ (see Fig. 7). Fortunately it appears that knowledge won from the model comparisons may indeed be relevant for more experimentally realistic ligands, since relative isomer energetics do not seem particularly sensitive to NH_3 versus imidazole as supporting ligands. Thus, at the BLYP/TZP level the bis(μ-oxo) isomers of $[(NH_3)_3Cu]_2O_2^{2+}$ and $[(imid)_3Cu]_2O_2^{2+}$ are predicted to be 8.4 and 8.3 kcal mol^{-1}, respectively, above the corresponding side-on peroxo isomers. At the B3LYP/TZP level (the hybrid functional now being the most appropriate), the end-on peroxo isomers are predicted to be 22.9 and 17.2 kcal mol^{-1}, respectively, above the corresponding side-on peroxo isomers. The BLYP prediction for this latter relative energy is 1.0 kcal mol^{-1}, indicating that the failure of pure functionals for this equilibrium continues to apply with the larger imidazole ligands, and the B3LYP prediction for the former equilibrium is 27.3 kcal mol^{-1}, indicating that the failure of the hybrid functionals for bis(μ-oxo) isomers is also preserved. So, the dark cloud is that different kinds of functionals are required for accuracy in different regions of the potential energy surface, but the silver lining is that lessons learned with small ligands appear to apply with larger ones.

Siegbahn has also advocated for the reasonably good mimicry of imidazole by ammonia provided intramolecular hydrogen bonding associated with the ammonia ligands does not become an issue [190], although he noted that in B3LYP calculations

of side-on peroxo isomers, broken-symmetry energies were very close to triplet energies with supporting imidazole ligands, but with ammonia ligands the broken-symmetry energies were substantially lower than triplet energies [96]. With respect to additional influences on imidazole-supported equilibria, Siegbahn and Wirstam [191], in some preliminary thoughts on the catalytic mechanism of tyrosinase, reported that coordination of neutral tyrosine to the $Cu_2O_2^{2+}$ core supported by six imidazole ligands had negligible influence on the relative energies of the side-on peroxo and bis(μ-oxo) isomers (as would be expected given the already full coordination shells about the copper atoms). Piquemal et al. [192] also noted that phenol coordination to the side-on peroxo system was inconsequential unless prior deprotonation to the phenoxide occurred.

Many other studies at the DFT level have been reported relevant to these equilibria. In an early study aimed less at exploring isomerization energetics per se and more at elucidating fundamental differences in electronic structure, Liu et al. [170] optimized the geometries of the singlet side-on peroxo and bis(μ-oxo) isomers of both $[(NH_3)_3Cu]_2O_2^{2+}$ and $[(NH_3)_2Cu]_2O_2^{2+}$ with the restricted B3LYP functional and an unpolarized all-electron double-ζ basis set. Single point calculations with the same functional but a polarized triple-ζ basis set indicated the side-on peroxo species to be 12.6 kcal mol^{-1} lower in energy than the bis(μ-oxo) form, but that energy dropped another 12.6 kcal mol^{-1} if the peroxo wave function was permitted to break spin symmetry (no spin purification was undertaken), consistent with other B3LYP results summarized here. Liu et al. also located a TS structure between the two minima and found it to be 17.0 kcal mol^{-1} above the peroxo isomer at the restricted B3LYP level and 28.8 kcal mol^{-1} at the unrestricted level. Analysis of the topologies of the electron density in the two isomers suggested that the two copper atoms cannot be said to be bonded one to another in the bis(μ-oxo) isomer and that the O–O bond is not fully broken in the TS structure (additional topological analysis of the B3LYP and CASSCF electron densities for bare $Cu_2O_2^{2+}$, $[(NH_3)_3Cu]_2O_2^{2+}$, and $[(imid)_3Cu]_2O_2^{2+}$, where imid = imidazole has been reported by Piquemal and Pilme [193], who noted that DFT and CASSCF densities agree with one another better as the number and size of ligands is increased).

Liu et al. [170] emphasized that when there are three ligands per copper atom, it is very important for the stability of the side-on peroxo and bis(μ-oxo) isomers, respectively, that the equatorial ligands be permitted to bend out of the plane of the $Cu_2O_2^{2+}$ core in the former and remain in the plane in the latter. Indeed, they found that neither minimum existed by their protocol if the equatorial ligands were constrained to adopt their geometric orientation about the core associated with the alternative isomer. They also noted the substantially weaker axial coordination associated with the bis(μ-oxo) form compared to the side-on peroxo, consistent with the known preferences of Cu(III) versus Cu(II) coordination compounds. Interestingly, they noted that the out-of-plane preference observed for the equatorial ligands in $[(NH_3)_3Cu]_2O_2^{2+}$ was entirely dependent on the presence of the third axial ligand—the ammonia ligands optimized to lie in the plane of the $Cu_2O_2^{2+}$ core for both isomers of $[(NH_3)_2Cu]_2O_2^{2+}$. Finally, they noted that an analysis of the Kohn–Sham orbitals along the reaction coordinate for isomerization of side-on peroxo to bis(μ-oxo) $[(NH_3)_3Cu]_2O_2^{2+}$ offered a mechanistic picture identical to that previously summarized by Cramer et al. [134] based on consideration of the HF orbitals as described in Section 3.2.1 above (a similar analysis was also done by Bérces based on BP86 orbitals [89]). Alvarez et al. [194] have discussed the generality of such an analysis for bridging ligands in dinuclear systems.

Metz and Solomon [195] also examined the $[(NH_3)_3Cu]_2O_2^{2+}$ case using B3LYP with the unpolarized LANL2DZ basis set. In this case, the authors were interested primarily in characterization of the reaction coordinate for binding O_2 when the copper atoms were constrained to distances relevant to those found in oxyhemocyanin. Within that context, using spin-purification to compute the singlet energies, Metz and Solomon found that the final, singlet, side-on peroxo structure was lowest in energy of all those considered, including an end-on peroxo triplet and μ-η^1:η^2-peroxo singlet implicated as intermediates in the binding process. This work extended upon prior studies on the oxygen-binding reaction that had either used lower levels of theory or less complete ligation of the copper atoms [55,196]. Interestingly, Metz and Solomon noted that the non-hybrid functional BP86 gave a stable restricted Kohn–Sham wave function for the side-on peroxo isomer of $[(NH_3)_3Cu]_2O_2^{2+}$, and they rejected further use of this functional as such behavior seemed inconsistent with the picture of one electron being localized on each copper atom in a di-Cu(II) system. This is a common misconception in the application of DFT to biradicals; proper singlet wave functions, like those from multireference calculations, for instance, have rigorously zero spin density at every position in space [126,138,148,162] so there is no a priori reason to distrust a stable restricted KS solution for a biradicaloid, although the model may fail to be appropriate for other reasons (see discussion in Section 3.1.2).

Indeed, in prior work Bérces [88] had employed the BP86 functional with polarized multiple-ζ basis sets to study the side-on peroxo/bis(μ-oxo) isomerizations of $[(TACN)Cu]_2O_2^{2+}$, $[(Tpz)Cu]_2O_2$, and $[(NH_3)_3Cu]_2O_2^{2+}$. In these three molecules, the side-on peroxo isomer was predicted to be more stable than the bis(μ-oxo) by 0.2, 2.9, and 11.7 kcal mol^{-1}, respectively (the last result is consistent with that from other non-hybrid density functionals, vide supra), and the activation energies for isomerization were predicted to be 7.9, 8.8, and 11.7 kcal mol^{-1}, respectively (thus, in the last case the TS structure was predicted to be very close to the bis(μ-oxo) structure). The isomerization energy computed for $[(TACN)Cu]_2O_2^{2+}$ is consistent with the experimental observation that core isomerization in this molecule has a lower energy than oxygenation of its monomeric precursor (*N*,*N*′,*N*″-trialkyl-TACN)Cu^+, which was measured to be 8.8 kcal mol^{-1} [14]. Bérces also computed the oxygen-binding energies of $[(TACN)Cu]_2O_2^{2+}$, $[(Tpz)Cu]_2O_2$, and $[(NH_3)_3Cu]_2O_2^{2+}$ to be −14.3, −44.0, and 38.2 kcal mol^{-1}, respectively, noting that the first number is in a range consistent with observed reversible binding and the last number, being positive, is an indication of the inadequacy of the hexa-ammonia

model for studying this quantity (however, Metz and Solomon [195] computed a binding enthalpy of O_2 to $[(NH_3)_3Cu]_2O_2^{2+}$ of -6.3 kcal mol^{-1} when solvation effects in dichloromethane were included, suggesting that the proportionately greater solvation free energy of the dicationic species relative to the monomer with such small ligands may act to compensate error associated with the model). A key conclusion of the pioneering study of Bérces was that ligand rigidity and charge could have significant influence on O_2 binding energies and isomerization energies primarily because of the significant differences in preferred geometries about Cu(I) precursor ions, side-on peroxo Cu(II) ions, and bis(μ-oxo) Cu(III) ions, as also emphasized later by Liu et al. [170] (vide supra). Bérces later extended his binding-energy analyses to supported tri- and tetra-copper O_2 complexes as well [197].

Additional work focusing on the influence of geometric constraints built into multidentate ligands on isomerization energetics (and ultimately reactivity) was reported by Lam et al. [92], who examined cores supported by R_3TACN, R = H, *i*Pr, and R_3TACD, R = H, Me, *i*Pr. Experimentally, *i*Pr$_3$TACN is known to exist in solution as a rapidly equilibrating mixture of side-on peroxo and bis(μ-oxo) isomers [16], while Me$_3$TACD is found exclusively in the bis(μ-oxo) form and *i*Pr$_3$TACD exclusively in the side-on peroxo form [92]. IMOMM calculations using B3LYP and a double-ζ basis set for the quantum subsystem defined as all atoms except the *N*-alkyl groups and a hybrid MM3/UFF force field for the full system gave rather poor quantitative agreement with experiment (for example, the bis(μ-oxo) isomer of Me$_3$TACD was predicted to be 21.5 kcal mol^{-1} above the side-on peroxo isomer (computed with a restricted formalism), in spite of the presence of the former and absence of the latter in experimental solution), but did permit qualitative explanation of differences between the TACN and TACD ligands associated with the larger cone angle of the latter and its greater flexibility with respect to variation in NCuN angles on passing from one isomer to the other. A particularly interesting feature of the side-on peroxo *i*Pr$_3$TACD isomer is that the axial Cu–N bonds at the two copper atoms are neither trans to one another (as is typical in TACN cases) nor do they eclipse one another (which tends to be another low-energy local minimum in unconstrained systems) but they are instead rotated 64° relative to one another; this rotation is attributed to steric interactions between the *N*-alkyl ligands based on the IMOMM calculations, which correctly predict significant rotation (44°) for the R = *i*Pr system.

Siegbahn [96] later also examined the Me$_3$TACD system with the B3LYP functional (treating the entire system with DFT). He reported that (i) improving the basis set (to doubly polarized triple-ζ quality), (ii) accounting for relativistic effects, (iii) including solvation effects, (iv) properly spin-purifying the broken-symmetry energy of the side-on peroxo isomer, and (v) using a lower-energy bis(μ-oxo) geometry than that had been found by Lam et al. reduced the energy difference between the two isomers to about 2 kcal mol^{-1}, albeit still incorrectly favoring the side-on peroxo isomer. Siegbahn suggested that the remaining error was about what might be expected for B3LYP, and that conclusion is indeed consistent with the results noted above based on thorough analysis of $[(NH_3)_3Cu]_2O_2^{2+}$ isomerism.

3.3. Multireference theories applied to model systems

In a very early study that was focused primarily on determination of spectral features associated with different possible coordination motifs, Maddaluno and Geissner-Prettre [198] performed small multireference CI calculations from 2 × 2 generalized valence bond (GVB) reference singlet wave functions and determined that, for bare $Cu_2O_2^{2+}$, the side-on peroxo coordination was preferred over *cis* end-on peroxo and μ-1,1-superoxo alternatives (each having been considered at one time as being relevant to the binding of O_2 in oxyhemocyanin). They noted that use of the GVB protocol (which is equivalent to a CAS(2,2) computation) reduced the energies of the resulting wave functions relative to their RHF counterparts by more than 3 eV, consistent with the strongly biradical character of the singlet state formed from the antiferromagnetic coupling of the two Cu(II) atoms. *Trans* end-on peroxo and bis(μ-oxo) isomers were not considered in this study. However, Eisenstein et al. [125] did examine these other isomers using a similar 2 × 2 GVB protocol. When the individual copper atoms were supported by 0, 1, 2, or 3 ammonia ligands, they predicted the side-on peroxo structures to be lower in energy than end-on peroxo structures (all of which were either *cis* or nearly linear, curiously) and they noted that with three ammonia ligands, eclipsed and staggered ligand arrangements were very similar in energy; a similar result was reported by Mahapatra et al. [71] (vide supra).

Eisenstein et al. also reported that 2 × 2 GVB optimizations beginning from the RHF/STO-3G bis(μ-oxo) structure reported by Mahapatra et al. [86] for $[(NH_3)_3Cu]_2O_2^{2+}$ led smoothly to the side-on peroxo structure, i.e., the bis(μ-oxo) structure was not stationary at the 2 × 2 GVB level; this was thus an early observation of the inadequacy of small active spaces in multireference calculations on supported $Cu_2O_2^{2+}$ cores. Finally, Eisenstein et al. noted that when each Cu atom was supported by four ammonia ligands, the end-on peroxo isomer was stable and exhibited geometric details similar to a known TMPA supported core of Jacobson et al. [199]; when side-on coordination was enforced, one ammonia ligand was observed to dissociate from copper, consistent with the notion that, because of the thermodynamic preference for side-on binding of O_2, end-on isomers are only favored by tetradentate ligands.

A somewhat larger (8,6) active space together with modest basis sets was employed for the study of partially optimized geometries of $Cu_2O_2^{2+}$, $[(NH_3)_2Cu]_2O_2^{2+}$, and $[(NH_3)_3Cu]_2O_2^{2+}$ by Bernardi et al. [200]. These authors reported enormous variations (as large as 90 kcal mol^{-1} in the bare core) in relative state energies on going from CAS to CASPT2 energies, and noted also that the CAS geometries were very poor, predicting peroxo O–O bond lengths of 1.6–1.8 Å. They reported similar instabilities in a different study examining geometries relevant to the oxygen-binding step [196].

An extremely thorough study at the CAS and CASPT2 levels was provided by Flock and Pierloot [201], who examined basis sets of varying size, active spaces of varying size up to (12,14),

and relativistic effects on the $[(NH_3)_3Cu]_2O_2^{2+}$ equilibrium. Flock and Pierloot reported that their CASPT2 calculations predicted the bis(μ-oxo) isomer to be 12.7 kcal mol^{-1} below the peroxo isomer, which was precisely contrary to B3LYP calculations, where the prediction (with their geometries) was for side-on peroxo to be 19.9 kcal mol^{-1} below bis(μ-oxo). Like Cramer et al. [134] previously, Flock and Pierloot noted the dramatic change in the contributions of dynamical and non-dynamical correlation effects along the isomerization coordinate: non-dynamical correlation is maximal for the biradical-like peroxo isomer while dynamical correlation is maximal for the bis(μ-oxo) isomer. Considering CASPT2 to be more likely to accurately balance these various correlation effects, Flock and Pierloot suggested that B3LYP was qualitatively incorrect, and the prevalence of the side-on peroxo isomer in oxyhemocyanin and oxytyrosinase must be attributed to protein steric effects or solvation or counterions [201].

However, subsequent work by Cramer et al. [157,158] examining active spaces of similar and still larger size, together with consideration of multiple states in the CASPT2 procedure, led to the conclusion that it was not possible to identify a practically accessible active space that was well balanced for both of these isomers, and that while B3LYP is quantitatively incorrect (because of inclusion of HF exchange, vide supra), it is qualitatively correct in predicting the side-on peroxo to be the lowest energy isomer. One warning sign that the CASPT2 energies may be unreliable can be seen in the data summarized in Figs. 10 and 11 above. For the energies of the bis(μ-oxo) isomer relative to the side-on peroxo for $[(NH_3)_2Cu]_2O_2^{2+}$ and $[(NH_3)_3Cu]_2O_2^{2+}$, the CAS level of theory predicts 3.7 and 29.8 kcal mol^{-1}, respectively. At the CASPT2 level, on the other hand, the predictions are −25.1 and −17.2 kcal mol^{-1}, respectively. Thus, the PT2 corrections are predicted to be 28.8 and 47.0 kcal mol^{-1}, and these are sufficiently large that suspicions about the adequacy of the reference wave function are raised. Comparison to CR-CC(2,3),D, MRCI, and pure DFT results confirms that the CASPT2 model fails here.

The case is worse with the end-on peroxo/side-on peroxo equilibrium. While the full coordinates are not shown in Figs. 10 and 11, the energies of the end-on peroxo isomers relative to the side-on alternatives in $[(NH_3)_2Cu]_2O_2^{2+}$ and $[(NH_3)_3Cu]_2O_2^{2+}$ are predicted to be 73.0 and 99.0 kcal mol^{-1}, respectively, at the CAS level (offscale in the figures) and −1.0 and 39.4 kcal mol^{-1}, respectively, at the CASPT2 level (shown as separate points in the figures). Thus, again, the PT2 correction is predicted to be very, very large, and the quantitative accuracies of the CASPT2 predictions are quite poor.

It appears that the $Cu_2O_2^{2+}$ core represents a particularly difficult challenge for multiconfigurational approaches because of the size and composition of the valence space. Nominally, the valence space is formed from the copper 4s and 3d orbitals and the oxygen 2s and 2p orbitals. Such a space is thus 32 electrons in 20 orbitals. In practice, a (32,20) space is potentially tractable, as there are only four virtual orbitals if all electrons are spin paired. However, this means that there is also rather little potential to account for electron correlation. If we imagine the copper atoms to be Cu(I), then they are d^{10}, and in order to correlate the 3d electrons a 4d shell should be included in the active space (the so-called "double-shell" effect). If this is the only change made, and it is probably the most important one, then one is faced with a (32,30) active space, and that is very far beyond anything that can presently be computed with standard CASSCF techniques.

An interesting alternative to the CAS formulation that *can* handle extremely large active spaces, and can in principle return full CI energies, is the density matrix renormalization group (DMRG) algorithm [202]. Marti et al. [203] recently reported application of the DMRG algorithm to the bis(μ-oxo)/side-on peroxo equilibrium and illustrated that an energy difference converged with respect to active space size could be obtained. As the adopted model did not account for dynamical electron correlation, the energy difference itself was not particularly accurate, but its convergence with respect to active space size coupled with the potential for this method to be extended to include dynamical electron correlation is certainly intriguing.

3.4. Modeling of experimentally characterized systems

Because of their comparison to model systems typically having ammonia ligands, some reports on experimentally characterized systems have already been summarized above in Section 3.2.2. In an additional recent contribution, Aullon et al. [100] explored the influence on the side-on peroxo/bis(μ-oxo) equilibrium of substituents at the third and fifth positions of the pyrazole rings in Tpz ligands supporting $Cu_2O_2^{2+}$. They found that 5-substitution had very minor influence (although sufficiently strong electron-donating or withdrawing character could manifest some influence) but substitution at the third position was more decisive because of the much greater proximity of such substituents on the equatorial pyrazole rings to the oxygen atoms in the bis(μ-oxo) isomer. Thus, a hydrogen bonding 3-substituent like amino pushed the equilibrium in favor of bis(μ-oxo) while the repulsive interactions associated with fluorine or trifluoromethyl 3-substituents had the opposite effect.

In a different system designed to probe specific ligand interactions with different cores, Aboelella et al. [117] studied the equilibrium shown in Scheme 1 (in experimental work, the open *ortho* positions of the *N*-phenyl groups carried isopropyl substituents). The thioether substituent was introduced into the ligand in an effort to stabilize a monocopper oxygen species, and in particular one in which O_2 is bound end-on to copper. However, calculations at the B3LYP/DZP level suggested that the lowest energy oxygenated monocopper adduct involved singlet side-on peroxo coordination. Experimentally, the monooxygenated species was observed to dimerize with unoxygenated Cu(I) monomer and to form exclusively the bis(μ-oxo) core. At the B3LYP/TZP level including continuum solvation effects, however, the side-on peroxo isomer is predicted to be 3.5 kcal mol^{-1} lower in energy than the bis(μ-oxo) isomer. This behavior is in error in the direction expected based on the model comparisons already discussed above, and the additional comparisons to experimental systems presented below. The pure BLYP functional, on the other hand, correctly predicts the bis(μ-oxo) isomer to be the lowest, by 12.8 kcal mol^{-1}. The 15.3 kcal mol^{-1} difference between B3LYP and BLYP is very

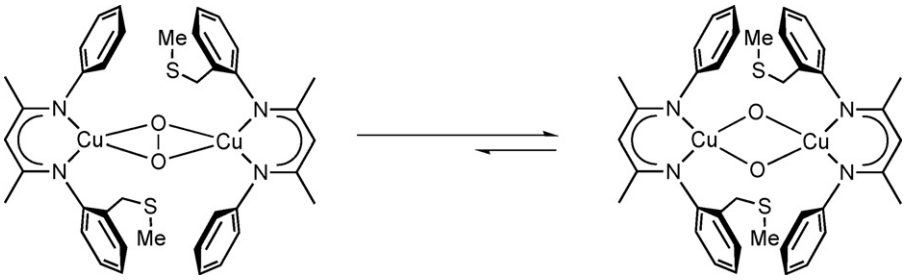

Scheme 1.

close to the magnitudes predicted for other analogous equilibria. In neither dimeric structure does the thioether coordinate to Cu.

As part of a study to understand the copper-catalyzed radical polymerization of phenol (vide infra), Tkatchouk et al. [3] examined the equilibrium between the bis(μ-oxo) and side-on peroxo forms of $Cu_2O_2^{2+}$ cores supported by TMEDA and *N*,*N*′,*N*″-trimethyl-TACN ligands at the PWPW91/DZP level including continuum solvation effects for toluene as solvent. They predicted both equilibria to favor the bis(μ-oxo) isomer, with the margin being larger for the bidentate TMEDA ligand (5.7 kcal mol^{-1}) than for the tridentate $TACN^{Me_3}$ ligand (0.4 kcal mol^{-1}), consistent with known experimental trends [12]. They additionally computed the TS structure energies for interconversion between the isomeric cores, predicting activation energies of 10.4 and 7.7 kcal mol^{-1} for the TMEDA and $TACN^{Me_3}$ ligands, respectively. Note the close agreement between the PWPW91 results of Tkatchouk at al. for $TACN^{Me_3}$ and those of Bérces for the unalkylated TACN ligand at the BP86 level discussed in Section 3.2.3 above, and their mutual agreement with experiment that the TACN systems should have equilibrium constants near 1. These results are consistent with both functionals being pure, i.e., incorporating no HF exchange.

The effect of coordinating an exogenous anion to a $Cu_2O_2^{2+}$ core supported by TEPD ligands at each copper was explored by Ottenwaelder et al. [113]. In a B3LYP/6-31G(d) broken-symmetry geometry optimization, the side-on peroxo structure was shown to be most stable and to exhibit a butterfly distortion (a dihedral angle of ∼150° between Cu_2O_2 planes) if the Cu–Cu distance was fixed at the corresponding experimental value of 3.51 Å [113]. A methane sulfonate anion was shown to bridge the two copper(II) ions through axial positions in this butterflied geometry, and it was concluded that this interaction imposed an electronic, as opposed to steric, preference for the side-on peroxo isomer.

The relative energies of the side-on peroxo and bis(μ-oxo) $Cu_2O_2^{2+}$ cores when supported by dinucleating ligands were explored by Company et al. through B3LYP/6-31G(d,p) calculations [105,109]. With a dinucleating hexaaza ligand, the bis(μ-oxo) isomer was determined to be 8.5 kcal/mol more stable than the side-on peroxo form [109]. Despite this energy difference possibly being underestimated due to the use of a hybrid functional, the result was in agreement with the experimental observation of solely the bis(μ-oxo) isomer [109].

Calculations on a Schiff-base variant of their hexaaza ligand [105] also predicted the bis(μ-oxo) to be most stable, this time by 4.8–8.5 kcal/mol, depending on the nature of the R group present on the spacer between the two triaza substructures of the ligand (see Fig. 5). The optimized geometries showed the imine N atoms remaining uncoordinated in the bis(μ-oxo) isomer, allowing greater flexibility to the ligand in this case and enhancing the ligand's stability relative to the conformation adopted in the side-on peroxo isomer. Ligand electronics were shown to play a role in the relative energy differences between isomers, as this quantity varied from smallest to largest for R = *t*Bu, CH_3, H, Cl, and NO_2 (the most electron-withdrawing substituent), respectively.

Costas et al. [106] examined the effects of steric and electronic factors on the nature of the $Cu_2O_2^{2+}$ peroxo isomer through calculations on a series of macrocyclic dinucleating ligands. Ligands were constructed using either Schiff-base components or substituted hexaaza components with varying numbers of methylenic units between the N donors (see Fig. 5). Interestingly, in nearly all cases the restricted singlet formulation of the side-on peroxo isomer proved to be most stable in BP86/DZP//VWN/DZP calculations. Hybrid functionals, such as B3LYP and BHLYP, which contain 20% and 50% HF exchange and might thus be expected to be more disposed to yielding stable broken-symmetry solutions (vide supra), *also* converged to restricted wave functions. The only exception noted by Costas et al. was for the most sterically demanding ligand containing the largest number of methylenic units between methyl-substituted N-donors. In this case, the triplet *trans* μ-1,2-peroxo isomer was the ground state with this preference being attributed to the ∼1.0 Å greater distance between Cu centers for this ligand, which leads to relatively weak dioxygen activation. Lastly, for the singlet side-on peroxo structures, the computed electrophilicity index [204] demonstrated a dependence on the nature and size of the macrocyclic ligands. In particular, the largest unsubstituted ligand cases yielded the smallest calculated electrophilicities.

A particularly broad survey of experimentally characterized side-on peroxo/bis(μ-oxo) equilibria has been carried out by Lewin et al. [93] examining in particular this issue of sensitivity of different density functionals to the inclusion of HF exchange; comparison to experiment provides a set of benchmark values different from the CR-CC standards used in the ammonia-supported model systems described above. Lewin et al. considered $Cu_2O_2^{2+}$ cores supported by the ligands in Fig. 12, for each of which some experimental data are available for the side-on peroxo/bis(μ-oxo) equilibrium. These experimental data range from measured enthalpies and entropies to less detailed observations of isomer ratios under various conditions. Shown in Fig. 12 are summaries of data for seven ligands and

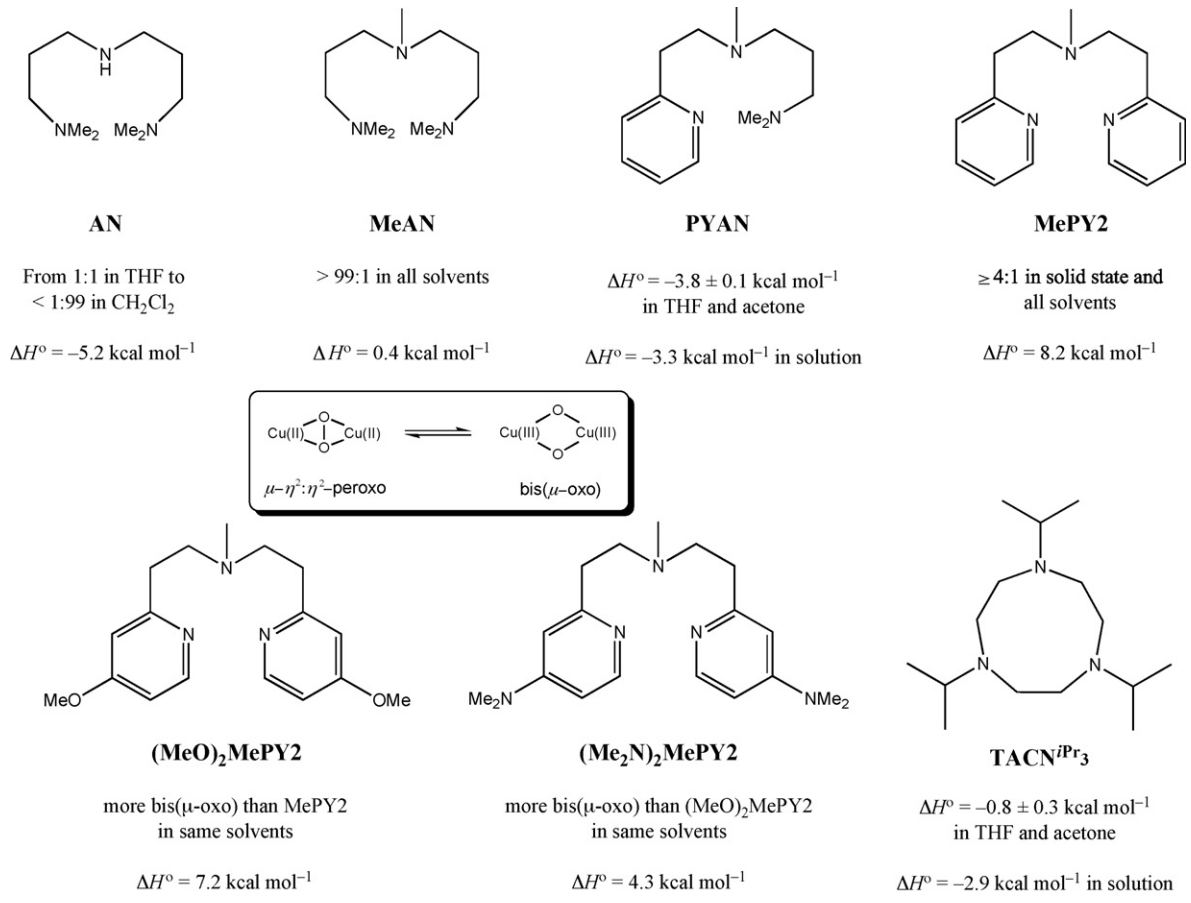

Fig. 12. Summary of experimental observations for the side-on peroxo/bis(μ-oxo) equilibrium with different ligands supporting copper (higher text below each ligand, sense of equilibrium is side-on peroxo:bis(μ-oxo)) and TPSS enthalpies of isomerization (lower text below each ligand, gas-phase unless otherwise noted) predicted by Lewin et al. [93].

results predicted by Lewin et al. with the pure TPSS functional and a hybrid basis set roughly polarized triple-ζ in quality in the core and decreasing in quality in more distant portions of ligands. Where quantitative results can be compared, the agreement is quite good, and in the remainder of cases the TPSS predictions are consistent with the experimental trends. The pure functionals BLYP and *m*PWPW91 provided identical results to within a few tenths of a kcal mol^{-1}.

As with the ammonia-containing model systems discussed above, however, Lewin et al. [93] found that the incorporation of HF exchange in hybrid functionals decreased the accuracy of the predicted isomerization energies. Specifically, hybrid functionals overstabilized the side-on peroxo isomer relative to the bis(μ-oxo) alternative by roughly 5–10 kcal mol^{-1} for each 10% of HF exchange incorporated into the functional (just the range noted above for the ammonia supported models). As with the smaller model systems, the side-on peroxo restricted KS wave functions for the different ligands were predicted either to be stable or weakly unstable with the pure functionals, but to be increasingly unstable with the hybrid functionals as increasing amounts of HF exchange were included.

Lewin et al. also performed implicit (continuum) solvent calculations to examine solvation effects on the equilibria, and predicted that solvation effects favored bis(μ-oxo) isomers in general by 1–4 kcal mol^{-1}, with larger ligands exhibiting reduced differential solvation effects. Analysis of molecular partition functions computed from analytic frequency calculations on the full experimental molecules indicated that the gas-phase entropies of isomerization were quite small, as might be expected. However, experimental measurements in solution typically indicate substantially larger entropies of isomerization. On that basis, Lewin et al. suggested that these entropies are likely to be primarily associated with changes in the "tightness" of interactions between molecular solutes and their first solvation shells.

4. Quantum chemical characterization of reactions of $Cu_2O_2^{2+}$ cores

The reactivities of supported $Cu_2O_2^{2+}$ cores have been characterized by many experimental studies and a number of recent reviews are available summarizing the scope of such reactions [10,20,21,36,37,77,83,205–208]. Rather than attempting to cover all known transformations, we will focus here on those reactions where theory has been brought to bear to further illuminate mechanistic details. The reactions in question primarily involve aromatic hydroxylation (because of special interest in this reaction as catalyzed by tyrosinase) and more general C–H bond activations, but certain other miscellaneous reactions are also discussed.

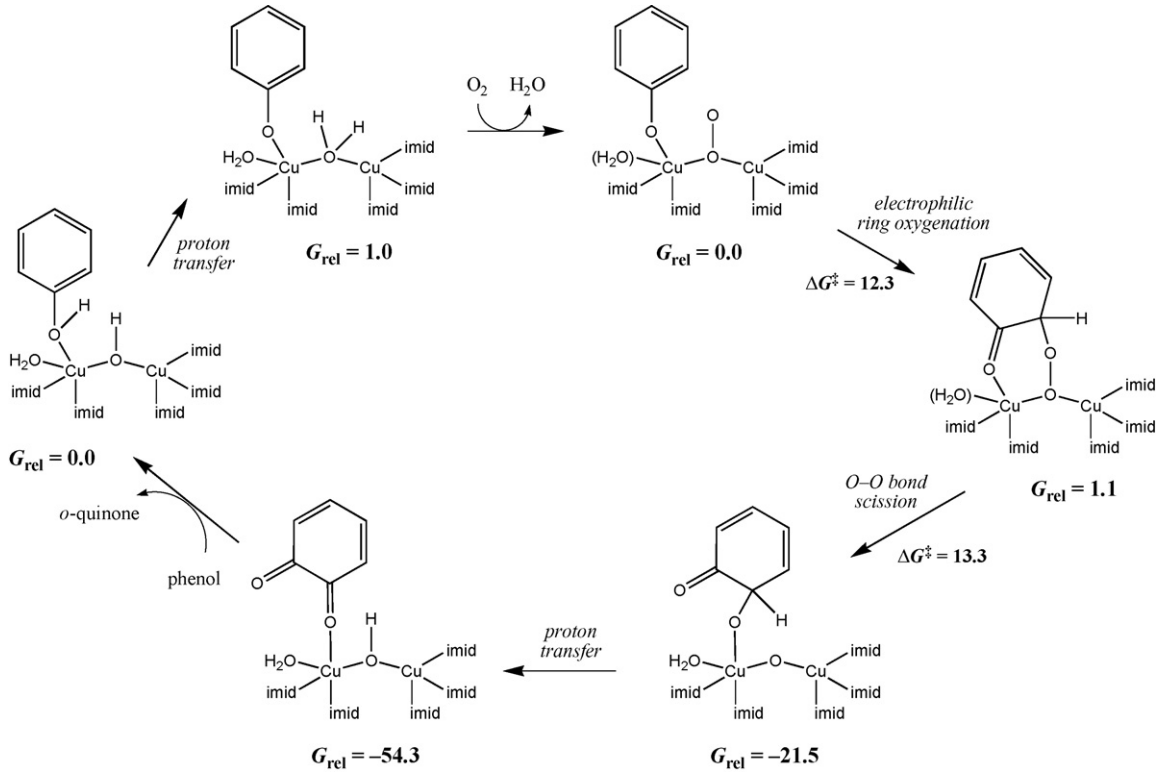

Fig. 13. Tyrosinase catalytic cycle proposed by Siegbahn based on B3LYP/TZP//B3LYP/DZP calculations including continuum solvation effects. All structures have a charge of +1; ligands in the second coordination shell are identified by placement in parentheses. Free energies are in units of kcal mol^{-1}.

4.1. Aromatic hydroxylation

Siegbahn [209] has examined the catalytic cycle associated with tyrosinase by modeling the aromatic hydroxylation of phenol by the $Cu_2O_2^{2+}$ core present in the enzyme active site, i.e., supported by six imidazole ligands (early work by Lind et al. [210] with less complete ligand analogs like ammonia and formaldimine was not useful as artifactitious hydrogen bonding interactions between individual ligands distorted structures and energies significantly). As shown in Fig. 13, Siegbahn began from a hydroxo-bridged dicopper(I) species with a coordinated phenol. Internal proton transfer followed by oxygenation generates the oxygenated dicopper intermediate in a roughly thermoneutral fashion (barriers along this portion of the cycle were not computed). The reactive complex was predicted to be coordinated in an interesting μ-1,1-superoxide fashion. Siegbahn found that this complex was so congested that reasonable TS structures for ring oxygenation could not be identified; he proposed dissociation of one ligand into the second coordination shell (either histidine or water, the latter being shown in Fig. 13) and identified a TS structure below the limit of roughly 13 kcal mol^{-1} that has been established from experimental rate studies [211]. Subsequent O–O bond scission with a barrier of similar magnitude was predicted. At this point, Siegbahn noted that B3LYP predicted a structure with a coordinated semiquinone radical to be substantially more stable than the coordinated quinone resulting from H transfer to the bridging oxo group. He speculated that properties of the enzyme active site might destabilize such a possible intermediate (which, if present, would serve as a thermodynamic sink shutting down the catalytic cycle). He also noted that B3LYP predicted an overall exothermicity 10 kcal mol^{-1} greater than that known experimentally, but suggested that QM/MM studies might help to resolve some of these discrepancies.

Siegbahn did not find a μ-η^2:η^2 oxygenated intermediate, like that known for the oxygenated resting state of the enzyme, with the coordinated phenolate. And, in earlier work, Siegbahn and Wirstam [191] argued against the possibility that a kinetically relevant mechanism for ring hydroxylation might also be available to the bis(μ-oxo) isomer. They based this argument on the high energy of a near-TS structure (a transit maximum not characterized by computation of the Hessian matrix) for proton transfer from the hydroxyl group of a coordinated phenol to one of the oxygen atoms of the bis(μ-oxo) core, like the first step shown in Fig. 13. As B3LYP was employed as the density functional for this study, one expects the studied bis(μ-oxo) isomers to be predicted to be too high in energy relative to side-on peroxo forms (vide supra). However, a more important issue with respect to the arguments of Siegbahn and Wirstam, as has been pointed out by Mirica et al. [112] (vide infra), is that there is no reason to believe that phenolic deprotonation in tyrosinase is accomplished intramolecularly by the $Cu_2O_2^{2+}$ core. Rather, it is as likely that proton transfer takes place to a basic residue in the active site of the enzyme. The more relevant computation of a ring oxygenation TS structure in an imidazole-supported bis(μ-oxo) core has not been accomplished. Based on B3LYP calculations, Siegbahn [96,212] has argued that the imidazole-supported bis(μ-oxo) core is intrinsically too high in

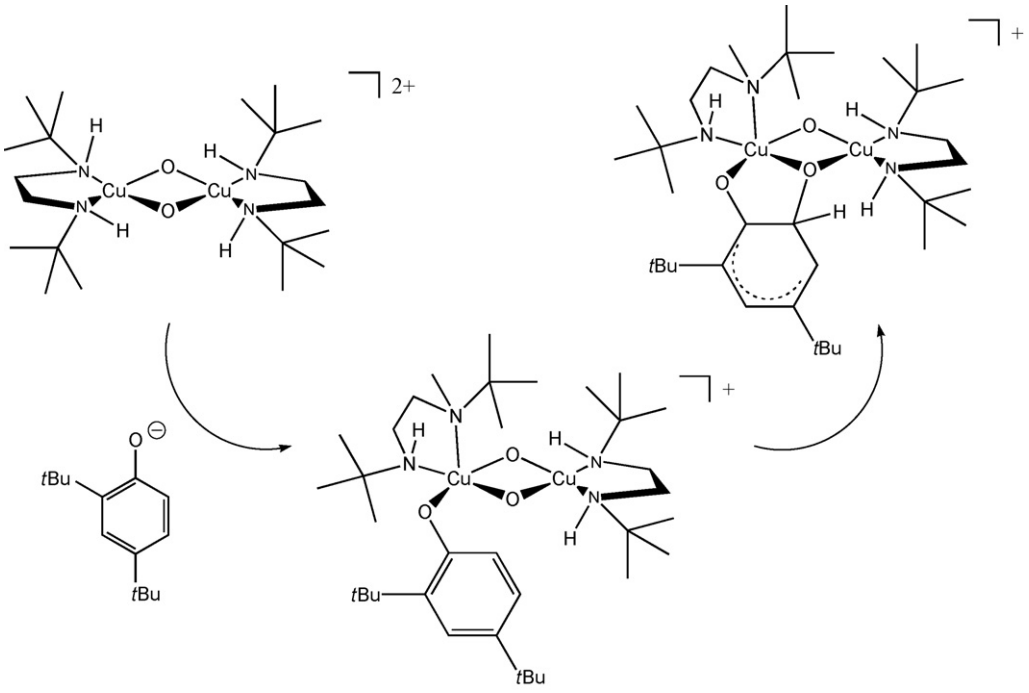

Scheme 2.

energy compared to the side-on peroxo isomer ever to be relevant, but the errors in the predicted energetics for this equilibrium introduced by HF exchange included in the B3LYP functional [157,158] may warrant additional consideration of this point. Of course, even if a kinetically reasonable pathway were found with free imidazole ligands, that would not necessarily imply that the enzyme active site is sufficiently plastic to support the smaller bis(μ-oxo) core; QM/MM studies including the enzyme would likely be necessary to address that point. Irrespective of the actual catalytic mechanism of tyrosinase, the kinetic competency of different cores with respect to C–H bond activation (whether aliphatic or aromatic) makes these systems particularly interesting for small-molecule catalyst design.

While they did not consider imidazole residues as ligands, Mirica et al. [112] *have* examined aromatic hydroxylation from a bis(μ-oxo) core. Thus, for the reaction shown in Scheme 2, Mirica et al. computed a gas-phase B3LYP/DZP activation energy of either 10.9 or 12.0 kcal mol^{-1} (the former value appears in the printed paper while the latter is listed in the methods section of the supporting information), which compares well to the measured value of 10.3 kcal mol^{-1} at −120 °C in 2-methyltetrahydrofuran. Mirica et al. note that coordination of the phenolate to the copper core occurs equatorially in the relaxed intermediate (irrespective of coordination to an axial or equatorial position in an initial geometry) and emphasize that this permits alignment of the aromatic π system with the LUMO of the electrophilic $Cu_2O_2^{2+}$ core (such a geometric preference was emphasized by Chen and Solomon [99] in a general analysis of HOMO/LUMO interactions that might influence the reactivities of side-on peroxo and bis(μ-oxo) $Cu_2O_2^{2+}$ isomers with both aryl and phosphine substrates). As already emphasized above, Mirica et al. note that the influence of a coordinating phenolate on the end-on peroxo/bis(μ-oxo) equilibrium has not been probed for the imidazole supported core present in tyrosinase, but if it were to lower the relative energy of the bis(μ-oxo) form – which is a reasonable hypothesis given the Cu(III) character of this isomer compared to Cu(II) for peroxo – then the low barrier to ring oxygenation might make this pathway kinetically relevant. A noteworthy feature of this calculation is that, if anything, the B3LYP model should predict the bis(μ-oxo) species to be too *high* in energy relative to side-on peroxo alternatives (because of incorporation of HF exchange, vide supra), so the question is indeed provocative.

Kinsinger [213] also examined the oxygenation of phenol by $Cu_2O_2^{2+}$ cores supported by various ligands (ammonias, nitriles, and imidazoles) at the *m*PWPW91/DZP level of theory. However, the propensity for pure functionals to overestimate the stability of end-on peroxo isomers compared to others led to most cores opening and reacting from end-on geometries at this level of theory. It thus remains something of a challenge to find a single theoretical protocol capable of characterizing the full potential energy surface for this reaction in a balanced way. Very recently, Naka et al. [102] reported a theoretical study of the oxidation of phenol to catechol by the μ-η^2:η^2-peroxo isomer of $(MePY2Cu)_2O_2^{2+}$. At the B3LYP/DZP level they found, like Kinsinger [213], that addition of phenolate to one copper led to an end-on peroxo species that then added to the ring in a subsequent electrophilic addition step. As hybrid functionals are better suited to modeling the end-on/side-on peroxo equilibrium, this provides greater support for the potential validity of this mechanism when the Cu atoms are supported by tridentate ligands.

4.2. General C–H bond activation

One of the first bis(μ-oxo) dicopper molecules to be reported, $(TACN^{Bn_3})Cu_2O_2^{2+}$, was found by Mahapatra et al. [87] to

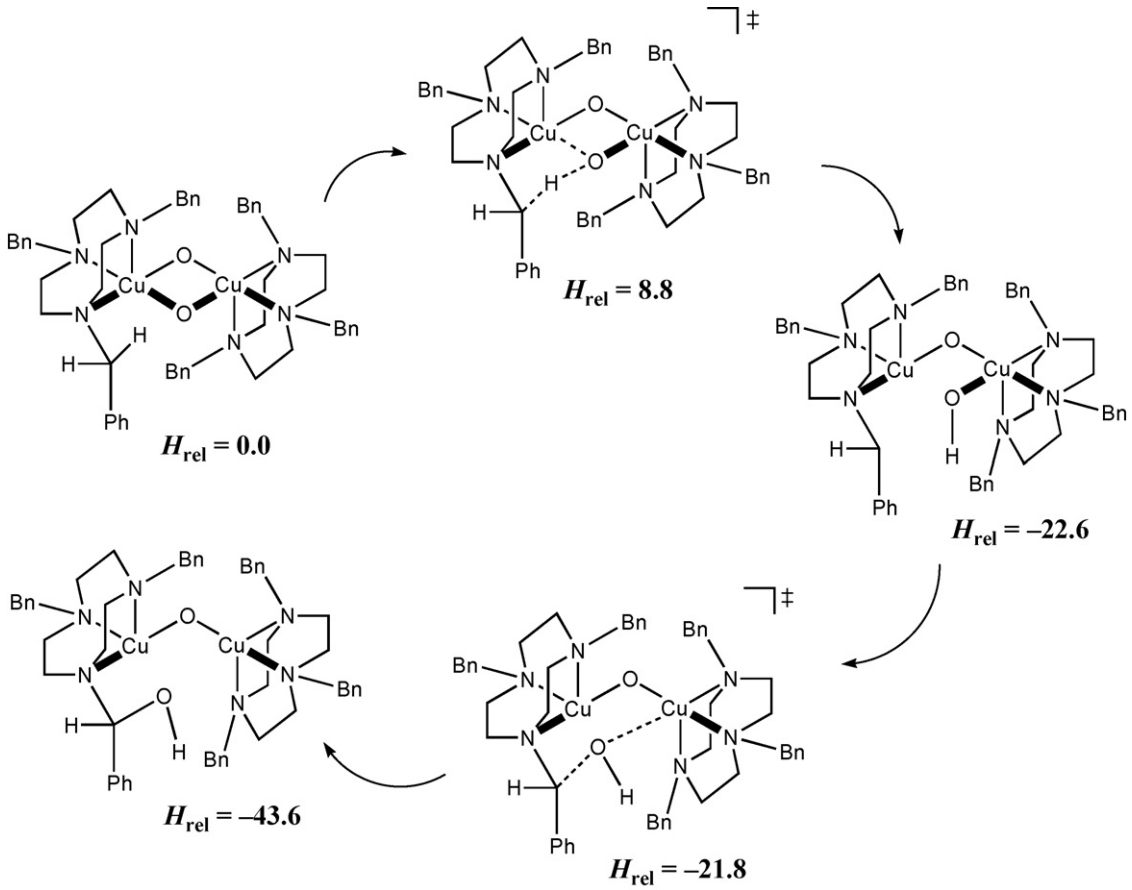

Fig. 14. Mechanism for benzylic oxidation of *N*-substituted TACN ligand by supported bis(μ-oxo) core (all species have charge 2+). Relative enthalpies are in kcal mol^{-1}.

decompose over time by unimolecular oxidation of a ligand-based benzyl group. Cramer and co-workers [90,91] studied this reaction using the IMOMM model of Morokuma and co-workers [128,214], treating the five unreactive benzyl groups exclusively with the universal force field (UFF; [215]) and modeling the remainder of the molecule at the MPW1K/DZP level (Fig. 14). The MPW1K functional was developed specifically for the accurate computation of H-atom transfer activation energies [216]. For comparison purposes, an analog with all benzyl groups replaced by methyl groups was modeled with the identical protocol.

As shown in Fig. 14, Cramer et al. found the first step to have a fairly low activation enthalpy leading to a μ-oxo-μ-hydroxo intermediate that is only very weakly stationary, requiring only 0.8 kcal mol^{-1} activation enthalpy to transfer the hydroxyl group back to the benzylic position. Calculations on models with *para* CF_3 and OH groups led to rate-determining activation enthalpies of 9.5 and 7.8 kcal mol^{-1}, respectively. These changes with substitution were qualitatively identical to those observed experimentally, but about twice as large in magnitude (possibly because the calculations did not include solvation effects, which tend to level such variations [125]). In addition, Cramer et al. predicted tunneling to play an important role in the kinetics of the reaction at the experimental temperatures. Using various one-dimensional tunneling models, H/D kinetic isotope effects (KIEs) from 24 to 61 were computed, which compared well with the experimental KIE of 40 ± 4 [87].

Spuhler and Holthausen [118] also modeled C–H activation at a ligand position, in this case for reaction of a $Cu_2O_2^{2+}$ core supported by *N*-ethyl-*N*-[2-(2-pyridyl)ethyl]-2-phenylethylamine ligands at each Cu [74]. Using a B3LYP/TZP//B3LYP/DZ protocol with continuum solvation for acetone, Spuhler et al. found the side-on peroxo species to be 2.3 kcal mol^{-1} above the bis(μ-oxo) form observed experimentally (given that B3LYP was used, the difference in energies is probably considerably higher). We note that this same computational protocol was later demonstrated by Mirica et al. [111], with the bidentate ligand DBED, to yield optimized geometries for a side-on peroxo isomer having key metrical parameters in excellent agreement with experimental values. With their full ligand system Spuhler and Holthausen [118] found the activation energy for H-atom abstraction from the benzylic position to be 12.7 kcal mol^{-1} and computed a H/D KIE of 27.9; these values compared well with experimental measurements of 12.7 kcal mol^{-1} (in the experimental case a *free* energy) and 35.4, respectively. Results from a model system with somewhat truncated ligands were in rather poor agreement, suggesting that steric interactions associated with the full ligand raise the H-transfer activation energy 8.5 kcal mol^{-1}. Thus, provided that steric

constraints do not limit access, it appears that the bis(μ-oxo) $Cu_2O_2^{2+}$ core is highly reactive for C–H bond activation. Interestingly, in the case studied by Spuhler and Holthausen, no μ-oxo-μ-hydroxo intermediate is predicted to exist—after the barrier for H-atom transfer is crossed, the incipient hydroxyl group rotates and snaps back to the benzylic position with a monotonic decrease in the molecular energy along the reaction coordinate.

Activation of the C–H bond of an external substrate by a bis(μ-oxo) $Cu_2O_2^{2+}$ was also considered by Chen and Chan in a modeling study of particulate methane monooxygenase (pMMO) reacting with methane [217]. This core, however, was less reactive than a trinuclear alternative proposed to be present in the enzyme active site. By contrast, Yoshizawa and Shiota [76] also considered the C–H bond activation of methane by pMMO, and suggested, based on QM/MM calculations that a bis(μ-oxo) $Cu_2O_2^{+}$ was competent for this process, i.e., a mixed-valence doublet Cu(II)Cu(III) species as opposed to a fully oxidized singlet dicationic core (Yoshizawa and Shiota also proposed that the third Cu atom in the enzyme active site could react with dioxygen to form a triplet Cu(III)O species capable of performing the oxidation).

Finally, as described in more detail in the next section, York et al. [116] have characterized the activation energies and reaction thermodynamics for H-atom transfer from 1,4-cyclohexadiene to $Cu_2O_2^{2+}$ and mixed-metal $CuMO_2^{+}$ bis(μ-oxo) cores, dissecting these energies into electron transfer and proton transfer components. Similar studies have also been done for monocopper O_2 complexes [218].

4.3. Redox reactions and proton transfers

Siegbahn [219] has examined the catalytic cycle of catecholase (Fig. 15) and found close similarities for certain key steps to those he proposed in his mechanism for tyrosinase [209] (vide supra). In the catecholase case the existence of X-ray crystal structural data permitted the model to be restrained to hold key atoms at positions relevant to the enzymatic active site, which was not true for the tyrosinase case. As in tyrosinase, the oxygenated reactive complex involves a μ-1,1-superoxide, but in this case the O_2 fragment acts as a base to abstract the remaining proton from the coordinated catecholate. Reduction of copper and dissociation of the product quinone leaves a hydroperoxo moiety that accepts another two protons from a new catechol; in the process the O–O bond is predicted to break, liberating one water molecule and regenerating a hydroxo bridge postulated to be present in the initial structure of the cycle. In addition to the cycle shown in Fig. 15, Siegbahn considered cycles having net charges of 0 and +2 (created by removing and adding one proton, respectively). In each case, the oxygenated intermediate was reported to adopt a side-on μ-η^2:η^2 peroxo motif, but otherwise similar catalytic cycles having similar energetics to those in Fig. 15 were said to be predicted.

Without regard to a particular catalytic cycle, a general study of protonation free energies, reduction potentials, and their combination to generate hydrogen-atom transfer free energies [220] has been reported by York et al. [116] in the context of a joint experimental/theoretical study of the reactivity of dicopper and mixed-metal bis(μ-oxo) cores (Fig. 16). Only the bis(μ-oxo)

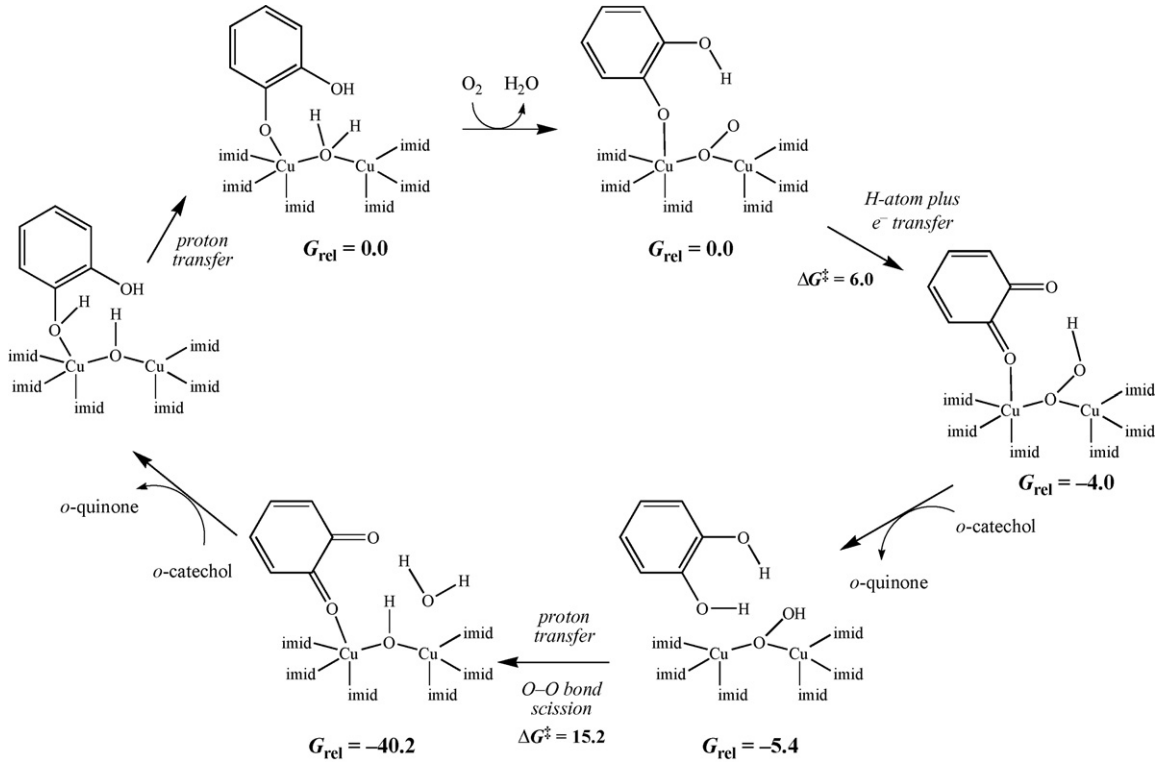

Fig. 15. Catecholase catalytic cycle proposed by Siegbahn based on B3LYP/TZP//B3LYP/DZP calculations including continuum solvation effects. All structures have a charge of +1. Free energies are in units of kcal mol^{-1}.

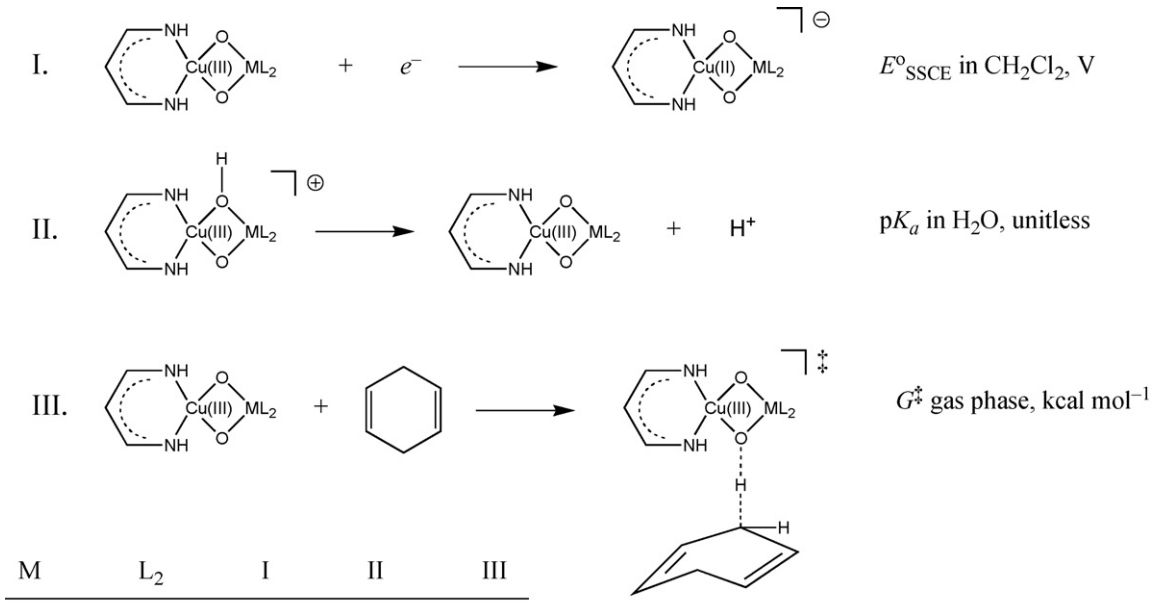

M	L_2	I	II	III
Cu	diketiminate	–1.99	9.5	17.4
Pd	2 Ph_3P	–2.19	15.7	17.8
Pt	2 Ph_3P	–1.86	14.0	18.9

Fig. 16. Reactions studied by York et al. [116] at the B98/TZP level of theory including continuum solvation effects for reactions I and II. See to right of reactions for units used in table at lower left.

isomers were observed with the experimental diketiminate and phosphine ligands. York et al. found that one-electron reduction occurred at the Cu(III) ion in the heterobimetallic systems, reflecting the greater electron affinity of Cu(III) compared to either Pd(II) or Pt(II). With respect to proton affinity, the heterobimetallic species were predicted to be more basic than the dicopper bis(diketiminate) and this result was consistent with their distinct reactivities with CO_2 and NH_4PF_6. Despite their reasonably high proton affinities, the systems were predicted to have large negative reduction potentials, consistent with their sluggish H-atom abstraction reactions with phenol to generate dimers from radical coupling. The relatively weak OH bonds that result from H-atom abstraction are responsible for activation energies of about 18 kcal mol^{-1} even from the very good H-atom donor 1,4-cyclohexadiene.

Tkatchouk et al. [3] also examined the oxidative polymerization of phenol by $Cu_2O_2^{2+}$ cores, considering both the bis(μ-oxo) and side-on peroxo isomers supported by TMEDA and $TACN^{Me_3}$ ligands. As already discussed in Section 3.4, they obtained quantitatively useful results for the equilibria between the two isomers at the PWPW91/DZP level. Tkatchouk et al. were primarily concerned with assessing the relative basicities and H-atom affinities of the different cores—they found H-atom transfer to the bis(μ-oxo) core from various phenols to be about 25 kcal mol^{-1} more favorable than to the corresponding side-on peroxo core (although, of course, isomerization of the side-on hydroperoxo product to the μ-hydroxo-μ-oxo product would result in the same net reaction). They found computed partial atomic charges to properly reflect the greater basicity of the oxo bridges compared to the side-on peroxo oxygen atoms and also the Cu(III) character of the bis(μ-oxo) copper atoms compared to the Cu(II) character of the side-on peroxo copper atoms.

4.4. Other reactions

The Glaser reaction, known for more than a century [221], involves the Cu(I) catalyzed oxidation of acetylenes to diacetylenes using molecular oxygen in aqueous solution. Fomina et al. [222] have proposed a reaction mechanism, based on modeling studies at the B3LYP/DZP level, that involves a bis(μ-oxo) intermediate stabilized by hydrogen bonding of the oxo groups to protonated amino groups displaced from coordination to copper by their protonation (Fig. 17). The bis(μ-oxo) core disproportionates following double proton transfer to generate two Cu(III) acetylides. The C–C coupling of these acetylides with concomitant reduction of Cu(III) to Cu(II) is predicted to be strongly exoergic, and the resulting Cu(II) species can also form an acetylide capable of C–C bond formation, regenerating the Cu(I) starting material. In the absence of hydrogen bonding between the protonated amino groups and the bis(μ-oxo) oxygen atoms, Fomina et al. computed formation of the bis(μ-oxo) core from the acetylide to be about 20 kcal mol^{-1} less favorable, and thus unlikely to occur (note that the values in Fig. 17 are energies, not free energies, so entropy costs would further destabilize the bis(μ-oxo) species).

Another reaction reported for the bis(μ-oxo) $Cu_2O_2^{2+}$ core supported by *N*-benzyl-*N*-ethyl-2-(2-pyridyl)ethylamine is oxygen atom transfer to sulfides RSR′ to generate corresponding sulfoxides [223]. Tkatchouk et al. [224] examined this reaction at the PWPW91/DZP level including continuum solvation ener-

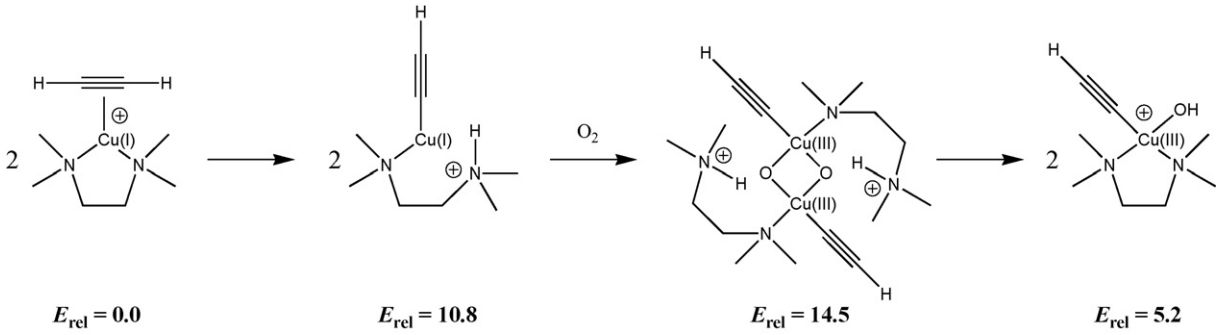

Fig. 17. Key steps in Glaser reaction mechanism involving a bis(μ-oxo) intermediate. Relative B3LYP/DZP energies with acetone continuum solvation effects are shown.

gies computed for acetone solution. In contrast to the originally proposed mechanism involving coordination of the sulfide sulfur atom to copper [223], Tkatchouk et al. found oxygenation to take place via direct insertion of the sulfide sulfur into a Cu–O bond of the bis(μ-oxo) core. Modest activation energies of about 7 kcal mol^{-1} were computed for the direct insertion process.

5. Quantum chemical characterization of key spectral features of $Cu_2O_2^{2+}$ cores

The spectral features associated with different $Cu_2O_2^{2+}$ cores and their ligands have been amply reviewed in the recent literature [12,20,22,36,37]. Therefore, this section focuses exclusively on theoretical contributions to rationalizing particular trends and observations without attempting to recapitulate the full range of experimental data. The primary spectral features of interest are associated with vibrational and resonance Raman spectroscopy in the infrared region of the spectrum, and electronic spectroscopy in the ultraviolet and visible region.

5.1. Resonance Raman and infrared vibrational spectroscopy

From analysis of photoelectron spectra for bare $Cu_2O_2^-$, Wang et al. [225] were able to assign a vibrational progression belonging to a totally symmetric mode of the rhomb-like geometry of *neutral* Cu_2O_2 having frequency $630 \pm 30\,cm^{-1}$. Based on computations at the BVWN/DZP level, these authors predicted harmonic normal modes at 182, 302, 466, 493, 653, and $718\,cm^{-1}$, with the final frequency being the totally symmetric stretch. Calculations by Holland et al. [226] for the *charged* core $Cu_2O_2^{2+}$ at the BPW91/DZP level predicted frequencies of 154, 204, 331, 377, 404, and $547\,cm^{-1}$. The significant decrease in each vibrational frequency is attributable in part to the Coulomb repulsion introduced in the rhomb by the double positive charge. Holland et al. also computed ^{18}O isotope effects, noting the largest effect ($28\,cm^{-1}$) for the highest frequency mode of the rhomb. We note here that the discussion of Holland et al. [226] incorrectly assigned the results of Wang et al. [225] to $Cu_2O_2^{2+}$, instead of Cu_2O_2.

The calculations of Holland et al. [226] extended to consideration of a number of supported bis(μ-oxo) $Cu_2O_2^{2+}$ cores as well, as illustrated in Fig. 18. Of particular interest to these authors was the effect of an asymmetric ligand environment on the observed resonance Raman spectra. The selection rules for the resonance Raman experiment dictate that only normal modes belonging to the totally symmetric irreducible representation (irrep) of the molecular point group benefit from resonance enhancement [227]. Such modes should also show depolarization ratios reduced from 0.75, while other modes should have exactly this value [228]. In the rhomb core of the bis(μ-oxo) isomer, two modes are of particular interest: a "breathing" mode, in which all atoms move, in concert, inward and outward relative to the center of mass, and a "pairwise" mode, in which the oxygen atoms effectively translate back and forth counter to one another along axes parallel to the Cu–Cu vector (Fig. 19).

In the highly symmetric cores, e.g., in $[(NH_3)_2Cu]_2O_2^{2+}$, the breathing mode belongs to the totally symmetric irrep and is observed in experimental analogs, while the pairwise mode belongs to another irrep, does not enjoy resonance enhancement, and is in general not observed. Reducing the symmetry of the ligand environment, e.g., as in $[(2\text{-aminomethylpyridyl})Cu]_2O_2^{2+}$, causes *both* of these modes to belong to the totally symmetric irrep of the lower symmetry point group, and in asymmetric experimental systems both modes are indeed typically observed, with isotope shifts and depolarization ratios consistent with those computed by Holland et al. Interestingly, Holland et al. found that with increased asymmetry, as in $[(NH_3)(HCN)Cu]_2O_2^{2+}$, for instance, the two modes mix in such a way that they cease to represent breathing and pairwise oxygen atom motion, and instead become more associated with coupled Cu–O stretches along the short and long Cu–O bonds, respectively, with increased depolarization ratios as a result (Fig. 19).

In order to estimate relative peak intensities, which should be proportional to the square of the normal mode displacements required to convert from the ground-state molecular geometry to that of the excited state in resonance with the electronic excitation [229], Holland et al. took the triplet-state geometry of $[(NH_3)(NF_3)Cu]_2O_2^{2+}$ to be a good analog for the lowest energy excited-state singlet, and found that motions along the breathing and pairwise normal modes required to convert from one geometry to the other were similar in magnitude, suggesting that the two modes should show roughly equal intensities, again consistent with experimental results.

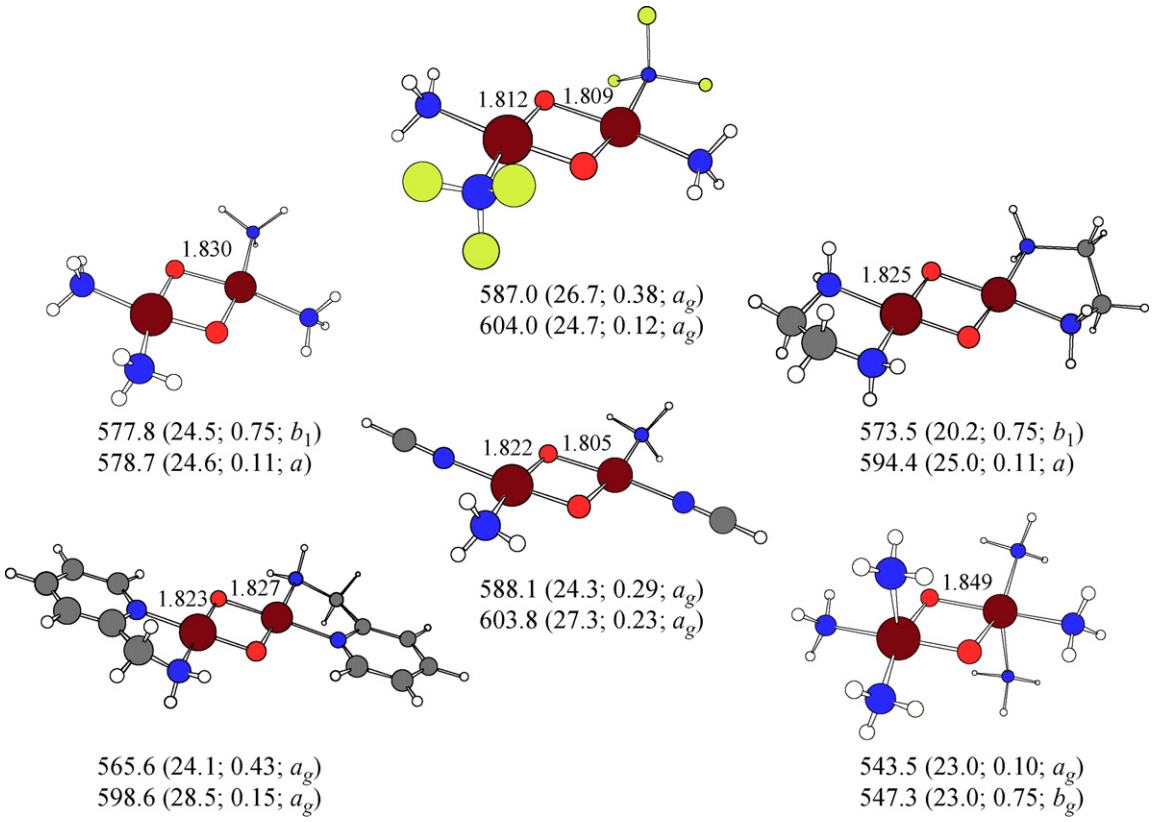

Fig. 18. Cu–O bond lengths (Å), key core vibrational frequencies (cm^{-1}), ($^{18}O_2$ isotope shifts (cm^{-1}); depolarization ratios (unitless); irreducible representation to which normal mode belongs) computed at the BPW91/DZP level for $[(NH_3)_2Cu]_2O_2^{2+}$, $[(NH_3)(NF_3)Cu]_2O_2^{2+}$, $[(EDA)Cu]_2O_2^{2+}$, [(2-aminomethylpyridyl)$Cu]_2O_2^{2+}$, $[(NH_3)(HCN)Cu]_2O_2^{2+}$, and $[(NH_3)_3Cu]_2O_2^{2+}$. Cu atoms, brown; F, mustard; O, red; N, blue; C, gray; H, white. (For interpretation of the references to color in this figure legend, the reader is referred to the web version of the article.)

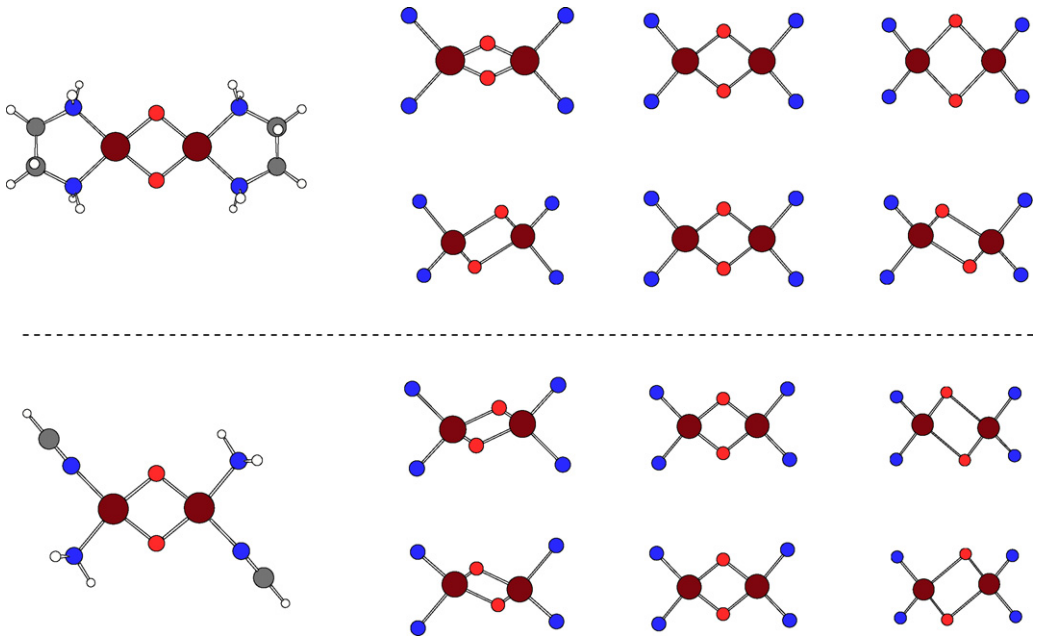

Fig. 19. Mixing of core normal modes (shown in reduced structures to right of molecules) with increasing ligand asymmetry illustrated by comparison of $[(EDA)Cu]_2O_2^{2+}$ to $[(NH_3)(HCN)Cu]_2O_2^{2+}$. For $[(EDA)Cu]_2O_2^{2+}$ (above the dotted line) the top and bottom normal modes are well described as breathing and pairwise vibrations. Cu atoms, brown; O, red; N, blue; C, gray; H, white. (For interpretation of the references to color in this figure legend, the reader is referred to the web version of the article.)

A complementary analysis of the resonance Raman spectra of bis(μ-oxo) cores was provided by Henson et al. [171] who carried out normal coordinate analysis of the 4-atom core with force constants optimized to reproduce observed frequencies in [(*N*,*N*′-diethyl-*N*,*N*′-dimethylcyclohexane-1,2-diamine)Cu]$_2O_2^{2+}$. In this case, Xα calculations were used to estimate the effect of electronic transitions on excited-state geometries since, as noted above, resonance Raman intensities are related to the overlap of individual normal modes with such distortions.

While the theoretical modeling of the bis(μ-oxo) cores has been particularly complete, there has been a substantial amount of work on other core isomers as well. Henson et al. [15] prepared a series of cores supported by H-, MeO-, and Me_2N-substituted pyridine-containing ligands and observed the effect of this variation in electron-donating capability on the O–O stretching frequencies in both end-on and side-on peroxo isomers (which have typical stretching frequencies of about 820 and 750 cm^{-1}, respectively). While they did not model their experimental molecules explicitly, they did analyze the side-on peroxo form of $[(NH_3)_3Cu]_2O_2^{2+}$ – varying the Cu–N distances to reflect stronger or weaker electron donation – in order to rationalize the lack of variation in side-on peroxo O–O stretching frequencies as a function of ligand substitution compared to end-on stretching frequencies, which varied over 15 cm^{-1}. Based on analysis of orbital amplitudes, Henson et al. concluded that in the side-on isomer there is a delicate balance between Cu–O_2 bonding via the in-plane π^*_{OO} orbital (depopulation of which increases the O–O stretching frequency) and Cu–O_2 back-bonding into the σ^*_{OO} (which decreases the O–O stretching frequency [56]) such that the effects of ligand substitution are precisely cancelled in the side-on isomer compared to the end-on alternative. Prior work in a similar vein by Baldwin et al. [230] explained the increase in the O–O force constant on going from an end-on monocopper superoxide to an end-on dicopper peroxide by noting that the new Cu–O bonding interaction decreased the population of the in-plane π^*_{OO} orbital, thereby increasing the O–O bond strength.

In addition to $Cu_2O_2^{2+}$ cores, some calculations of resonance Raman data for mixed $CuMO_2^+$ (M = Pd, Pt) cores have been reported [116,231]. Results are of similar quality to those for dicopper cores. Substantial theoretical characterization of monocopper–O_2 vibrational spectra has also been reported [232–234].

5.2. UV/vis spectroscopy

UV/vis spectroscopy has been particularly useful in the study of supported $Cu_2O_2^{2+}$ cores because of the sensitivity of the analytical technique and the diagnostic absorptions associated with different core motifs in this region of the spectrum. Moreover, these spectral signatures lie in regions that are not obscured by protein absorptions, so substantial early insights into relevant metalloenzymes were obtained using UV/vis spectroscopy.

5.2.1. Biological systems

Experimentally obtained UV/vis spectra for metalloenzymes containing $Cu_2O_2^{2+}$ cores have been described in detail in several review articles [9,10,21,22,37]. With small variations, the main features which occur in the UV/vis spectra for each one of oxyhemocyanin [28,235], oxytyrosinase [50], and oxycatechol oxidase [236] are an intense band ($\varepsilon \approx 20{,}000\ M^{-1}\ cm^{-1}$) at approximately 29,000 cm^{-1} (345 nm) and a weak band ($\varepsilon \approx 1000\ M^{-1}\ cm^{-1}$) at approximately 17,000 cm^{-1} (580 nm) (Table 1). These bands have been interpreted as charge-transfer transitions from the bridging side-on peroxide to the Cu(II) centers in the symmetric $Cu_2O_2^{2+}$ core [28]; the higher-energy band has been assigned to derive from promotion of an electron from the π* orbital of the peroxide moiety that is in the plane of the core, denoted π^*_σ, while the lower energy band has been assigned to derive from promotion of an electron from the π* orbital that is perpendicular to the plane of the core, denoted π^*_v (vide infra). In the particular case of oxytyrosinase, weak bands in the 700–800 nm region have also been recognized and assigned as d → d transitions within the tetragonal Cu(II) centers [28,235].

The earliest calculations of these UV/vis spectra were those of Maddaluno and Geissner-Prettre [198] who, using a planar μ-η^2:η^2-peroxo $Cu_2O_2^{2+}$ bare core as a model, computed UV/vis absorption energies based upon orbitals from two-reference-

Table 1
Absorption bands in the UV/vis spectra of systems with the μ-η^2:η^2-peroxo $Cu_2O_2^{2+}$ core (planar geometry unless otherwise noted)

Molecule	Theory	$\pi^*_\sigma \rightarrow$ Cu(II) CT	$\pi^*_v \rightarrow$ Cu(II) CT	Reference
Oxyhemocyanin	n/a	28,600–29,000 (~20,000)	17,200–17,500 (~1000)	[28,235]
Oxytyrosinase	n/a	29,000 (~17,000)	17,000 (~1000)	[50]
Oxycatechol oxidase	n/a	29,000 (strong)	17,400 (weak)	[236]
$Cu_2O_2^{2+}$	ROHF-GVB	63,600	43,900	[198]
$[(NH_3)_2CuO_2Cu(NH_3)_2]^{2+}$	SCF-Xα-SW	33,700–66,800[a]	16,000–17,800[a]	[54,55]
$[(NH_3)_2CuO_2Cu(NH_3)_2]^{2+}$	SCF-Xα-SW	44,330	19,520	[237]
$[(NH_3)_2CuO_2Cu(NH_3)_2]^{2+}$ (butterfly)	SCF-Xα-SW	43,160	26,845	[237]
$[(NH_3)_2CuO_2Cu(NH_3)_2]^{2+}$	VBCI	41,060	18,440	[136]
$[(NH_3)_3CuO_2Cu(NH_3)_3]^{2+}$	Gradient-corrected LDA DFT	61,200	37,500	[89]
$[(NH_3)_3CuO_2Cu(NH_3)_3]^{2+}$	TD-DFT (B3LYP)	28,050	15,970	[195]
$[(imid)_3CuO_2Cu(imid)_3]^{2+}$ (butterfly)	INDO/S	36,300	17,800	[238]

Energies given in cm^{-1} and absorption coefficients in parentheses in $M^{-1}\ cm^{-1}$.
[a] Range corresponds to values obtained with different copper sphere radii in the SCF-Xα-SW calculations.

determinant closed-shell SCF (ROHF-GVB) calculations. Their calculated values for the absorption bands were 63,600 and 43,900 cm^{-1}. The poor quantitative agreement with experiment was attributed to neglect of the contribution of the imidazole ligands to the UV/vis spectrum. On the other hand, the long wavelength absorption *was* calculated to have the weaker intensity and analysis of the leading contributions to the two transitions confirmed that the bands corresponded to $O_2 \rightarrow Cu$ charge transfers. Also consistent with experimental data [199], the calculated transition energies shifted to longer wavelengths with increased Cu–Cu distances. This effect was found to be most pronounced for the higher energy absorption.

Ross and Solomon added a degree of sophistication to the model by employing two NH_3 ligands per copper in addition to the μ-η^2:η^2-peroxo $Cu_2O_2^{2+}$ core [54,55]. The computations in this case used the spin-unrestricted SCF-Xα-Scattered Wave (SCF-Xα-SW [140,239–243]) methodology supplemented by the Slater transition-state method for determining the energies of the electronic transitions. The Slater model has the advantage of approximately accounting for the effects of relaxation due to changes in the electron density distribution in the excited state. While the low-energy band was accurately reproduced (with an error $\leq$1200 cm^{-1}), the more intense feature was predicted to be from 5000 to 37,000 cm^{-1} too high depending on the radius of the copper sphere in the SCF-Xα-SW computations.

The work from Ross et al. was the first to provide insight into the precise nature of these electronic transitions. The peroxide dianion moiety itself has a doubly degenerate set of valence π* orbitals which split in energy upon binding to the copper centers into in-plane σ-bonding and out-of-plane (vertical) π-bonding orbitals. Thus, two charge-transfer transitions are predicted from peroxide to the highest energy singly occupied d orbital on Cu(II). The low-wavelength, high-intensity band is an in-plane peroxide $\pi^*_\sigma \rightarrow$ Cu(II) charge-transfer transition and the high-wavelength, low-intensity band is an out-of-plane peroxide $\pi^*_v \rightarrow$ Cu(II) charge transfer [28]. These ligand-to-metal charge-transfer bands can also be used as a measure of the π^*_v–π^*_σ splitting, which provides a measure of the ligand–metal bonding contributions to the electronic structure. This in turn can be used to extract geometric information based upon the relationship between the geometry of the copper–peroxide bond and the π^*_v–π^*_σ splitting.

Later work from the same group extended these computations to investigate the difference in computed absorption spectra for planar and butterflied side-on μ-η^2:η^2-peroxo geometries [237]. Although the energy of the $\pi^*_\sigma \rightarrow$ Cu(II) charge transfer was predicted to change minimally as a function of the butterfly distortion, the intensity of the transition decreased with bending of the core due to reduced in-plane overlap between the π^*_σ and the Cu(II) d orbitals. In contrast, the $\pi^*_v \rightarrow$ Cu(II) charge transfer increased by ~7000 cm^{-1} on going to the butterfly core.

The broken-symmetry formalism employed in these SCF-Xα-SW calculations introduced complications as a consequence of being a single-determinantal method. The transitions from the broken-symmetry ground state to the mixed-spin excited states were computed as transitions to an average of excited-state components [244]. The large antiferromagnetic exchange interaction in the $\pi^*_\sigma \rightarrow$ Cu(II) charge-transfer excited state consequently explained the overestimation of this calculated transition. In the $\pi^*_v \rightarrow$ Cu(II) charge-transfer excited state, no bonding interaction occurred between the unpaired ligand electron and the unpaired electron on the metal, translating to a lack of antiferromagnetic coupling and resulting in good agreement with the experimentally observed values.

By combining the valence bond configuration interaction (VBCI) model with SCF-Xα-SW molecular orbital calculations, Tuczek and Solomon [136] were able to address this limitation. The antiferromagnetic interaction in the excited π^*_σ charge-transfer state was computed to be 29,800 cm^{-1}, and inclusion of this effect led to a lower prediction for the high-energy UV/vis band of 41,060 cm^{-1}. While this value remains 12,000 cm^{-1} higher than the experimental value for the $\pi^*_\sigma \rightarrow$ Cu(II) charge-transfer transition (cf. Table 1), it is nonetheless a marked improvement (~25,000 cm^{-1}) over the 66,800 cm^{-1} computed using the same Cu sphere radius with the pure SCF-Xα-SW methodology [54,55]. Examination of the excited-state antiferromagnetism, when correlated by the VBCI method to shifts in the charge-transfer transitions involving the peroxide ligand, also serves as a probe of the superexchange pathway in these $Cu_2O_2^{2+}$ systems.

The first application of DFT to prediction of the UV/vis spectrum of the side-on μ-η^2:η^2-peroxo motif for the $Cu_2O_2^{2+}$ core came from Bérces, who utilized a model with three ammonia ligands per copper center [89]. Gradient-corrected LDA density functional calculations with electronic excitation energies calculated according to the sum method of Ziegler et al. [139] led to predictions of 61,200 and 37,500 cm^{-1} for the in-plane π^*_σ and out-of-plane π^*_v charge-transfer transitions, respectively. The calculations are approximately double the experimental values measured in the metalloenzyme systems and were noted to suffer from a lack of configuration interactions in the methodology.

Calculations for the same model system using broken-symmetry DFT with the B3LYP functional combined with TD-DFT (time-dependent density functional theory) to determine the absorption spectrum proved more successful [195], in part due to the ability of TD-DFT to describe excitations with significant two-electron character [245]. The main features of the experimental spectra were reproduced: (1) an intense $\pi^*_\sigma \rightarrow$ Cu(II) charge transfer at 28,050 cm^{-1}, (2) a weak absorption at 15,970 cm^{-1} with mixed character ($\pi^*_\sigma \rightarrow$ Cu(II), $\pi^*_v \rightarrow$ Cu(II), and d → d), and (3) d → d transitions at 14,340 cm^{-1}. The computed value for the pure $\pi^*_v \rightarrow$ Cu(II) charge-transfer band of 6,310 cm^{-1} was however too low in energy, as the copper orbitals were overly stabilized relative to the ligand orbitals. This in turn reduced the $\pi^*_v \rightarrow$ Cu(II) character in the ~16,000 cm^{-1} band.

The UV/vis spectroscopy of the μ-η^2:η^2-peroxo $Cu_2O_2^{2+}$ core has been examined as well using the INDO/S methodology [246–248] at the configuration interaction singles (CIS) level of theory. In this work from Estiú and Zerner [238], the coordination environment consisted of three imidazole ligands per copper center. Estiú and Zerner, noting that the features in the experimental UV/vis spectra for oxyhemocyanin orig-

inated from transitions involving primarily the copper(II) ions and the peroxide group, used this fact to obtain detailed structural and electronic characteristics of the μ-η²:η²-peroxo $Cu_2O_2^{2+}$ core. The geometry yielding the best agreement between calculated and experimental UV/vis spectra occurred for a Cu–Cu distance of 3.76 Å and an out-of-plane O_2 height (butterfly distortion) of 0.05 Å. The low-energy band was computed to be located at 17,800 cm^{-1}, in good agreement with experiment. The 6000 cm^{-1} overestimation for the high-energy band (cf. Table 1) represented an improvement over both VBCI theory [136] and SCF-Xα-SW calculations [54,55]. Shorter distances between the copper centers led to calculated charge-transfer bands too high in energy due to overstabilization of the π_v^* orbital through mixing with the copper d orbitals. In addition, a planar core proved inadequate as the lower energy band in this case could not be assigned as a $\pi_v^* \rightarrow$ Cu(II) charge transfer since the former orbital does not overlap efficiently with the HOMO centered on the copper atoms. Variances in absorption spectra calculated for a range of Cu–Cu distances and butterfly distortions indicated the difficulty in determining whether spectroscopic variations among hemocyanin species [235] could be definitively attributed to one or the other of these structural differences. Lastly, Estiú et al. noted little difference in the energy of the transitions when localized reference states (i.e., an antiferromagnetic reference) versus delocalized reference states (i.e., restricted wave functions) were used in the calculations; computed oscillator strengths, on the other hand, favored the antiferromagnetic ground state.

5.2.2. Synthetic systems

The absorption spectrum for the end-on *trans* μ-1,2-peroxo motif was calculated by Baldwin et al. [230] using the SCF-Xα-SW method [140,239–243] for a system with four ammonias ligated to each copper atom, yielding a trigonal bipyramidal geometry at the metal centers. Computed values of ~13,000 and ~35,000 cm^{-1} for the $\pi_v^* \rightarrow$ Cu and $\pi_\sigma^* \rightarrow$ Cu charge-transfer transitions, respectively, were predicted compared to an experimental UV/vis spectrum having bands at 16,250 and 19,100 cm^{-1} for a biomimetic model complex supported by the tris(2-methylpyridyl)amine (TMPA) ligand with the same end-on *trans* core geometry [230]. The calculated covalency of the metal–ligand interactions resulted in the π_σ^* charge transfer being highly dependent on the copper sphere radius employed in the SCF-Xα-SW calculations [55]. As in the case of Ross and Solomon who performed similar calculations on a μ-η²:η²-peroxo $Cu_2O_2^{2+}$ core [54,55], the deviation of the calculated $\pi_\sigma^* \rightarrow$ Cu band from the experimental value was attributed to the limitations of using a single-determinantal formalism. In this limit, the excited state involved in the charge transfer is treated as an average of the possible mixed-spin mixed-symmetry excited state components. Strong coupling between the two sides of the dimer in the π_σ^* excited state therefore leads to a large deviation from the experimental value, while the error is significantly smaller for the π_v^* excited state, where the coupling is much weaker.

SCF-Xα-SW calculations were additionally used to elucidate the absorption spectrum of the bis(μ-oxo) $Cu_2O_2^{2+}$ core structure in which each copper was coordinated to two ammonia ligands [171]. Experimental UV/vis spectra of bis(μ-oxo) cores supported by a variety of synthetic ligands show bands at ~22,000–26,000 cm^{-1} (ε = 13,000–28,000 $M^{-1}\,cm^{-1}$) and ~31,000–34,000 cm^{-1} (ε = 11,000–21,000 $M^{-1}\,cm^{-1}$) [14,71,72,86,110,249,250]. Assignments for these bands were achieved by predicting the absorption coefficients and the relative oscillator strengths, computed using the Ros–van der Avoird method [251], for different charge-transfer transitions among frontier molecular orbitals. The low-energy band, with a computed energy of 30,090 cm^{-1}, was assigned as the transition from a MO formed from a bonding interaction between Cu d_{xy} orbitals and the oxygen $p_y + p_y$ antibonding orbital (σ_u^*) to a MO formed from an antibonding interaction between Cu d_{xy} orbitals and the oxygen $p_x - p_x$ antibonding orbital (π_σ^*). The high-energy band, with a computed energy of 59,895 cm^{-1} (an overestimation of ~28,000 cm^{-1}), was assigned as the transition from a MO formed from a bonding interaction between Cu d_{xy} orbitals and oxygen π_σ^* orbital to a MO formed from an antibonding interaction between Cu d_{xy} orbitals and the oxygen σ_u^* orbital. Notably, for both transitions, the acceptor orbitals are primarily Cu d in character whereas the donor orbitals have a relatively larger percentage of O p orbital character mixed with the Cu d orbital contributions. That the two lowest energy holes are metal based is consistent with the +3 oxidation state of the copper centers. Upon incrementing the copper coordination number to 5 by the addition of one ammonia ligand per copper center, the computed energies of the low- and high-energy bands shifted lower by ~2200 and ~3300 cm^{-1}, respectively. This perturbation was consistent with that observed upon increasing coordination numbers in the synthetic ligand systems [71,72,110,249,250]. Computations also revealed the low-energy band to be most sensitive to the $Cu_2O_2^{2+}$ core geometry and the high-energy band to be most sensitive to the metal coordination number.

Estiú and Zerner [238] likewise calculated the absorption spectra for the bis(μ-oxo) $Cu_2O_2^{2+}$ core, using their INDO/S methodology [246–248] and a model consisting of three imidazoles per copper center. Their computations yielded values of 22,000 and 28,000 cm^{-1} for the low- and high-energy bands in the bis(μ-oxo) spectrum, both of which were assigned to oxygen $\pi_v^* \rightarrow$ Cu(d_{xy})–O(p_y) charge-transfer transitions. The transition energies here represent a closer agreement with the experimental UV/vis spectra than that obtained from the SCF-Xα-SW calculations [171]. By comparing complexes with ammonia and imidazole ligands, Estiú et al. moreover determined that predicted absorption energies and intensities for the bis(μ-oxo) isomer were more strongly influenced by the ligands attached to the copper atoms than were those for the side-on μ-η²:η²-peroxo isomer.

Computations of the absorption spectra of $Cu_2O_2^{2+}$ cores supported by synthetic ligands are far less common. Bérces has used density functional theory to determine the electronic excitation energies (according to the sum method of Ziegler et al. [139]) of a side-on μ-η²:η²-peroxo geometry with the TACN ligand [89]. The calculated values of 65,200 and 36,000 cm^{-1} for the in-plane π_σ^* and out-of-plane π_v^* to copper charge-transfer

transitions, respectively, were close to those also determined by Bérces [89] for the analogous $[(NH_3)_3Cu_2O_2]^{2+}$ system (vide supra), which were approximately twice as large as the experimentally determined transitions.

6. Summary and conclusions

Quantum mechanical calculations have played a key role in characterizing the structure, spectroscopy, and reactivity of molecules containing supported $Cu_2O_2^{2+}$ cores. Because of the large number of electrons that must be correlated, multireference descriptions have been of limited use. Density functional theory has proven to have greater applicability, however, different core geometries show different sensitivities to the incorporation of Hartree–Fock exchange in hybrid HF-DFT functionals, varying as a function of the degree of singlet biradical character in the core. Such biradical character is associated with an antiferromagnetically coupled Cu(II)Cu(II) formulation. Thus, comparisons of bis(μ-oxo) energies to side-on peroxo energies are best made using pure functionals containing no HF exchange, while comparisons of side-on peroxo energies to end-on peroxo energies are best made with hybrid functionals. Obviously, this makes studies of large portions of potential energy surfaces challenging and the $Cu_2O_2^{2+}$ cores should be useful for the testing of future functionals as they are developed.

Modeling the spectroscopy and reactivity of $Cu_2O_2^{2+}$ cores is subject to the usual considerations associated with various theoretical methods [126], but poses no additional pathologies beyond the one just noted. As such, theoretical methods should continue to prove quite useful for relating structure to spectra, and for guiding experimental ligand design for the tailoring of specific properties and reactivity.

Acknowledgments

We gratefully acknowledge support for this work from the National Science Foundation (CHE-0610183). Professor Bill Tolman is also thanked for many a wise insight.

References

[1] N. Duran, E. Esposito, Appl. Catal. B 28 (2000) 83.
[2] G.F.Z. da Silva, W.M. Tay, L.-J. Ming, J. Biol. Chem. 280 (2005) 16601.
[3] E. Tkatchouk, L. Fomina, L. Rumsh, S. Fomine, Macromolecules 36 (2003) 5607.
[4] C. Limberg, Angew. Chem. Int. Ed. 42 (2003) 5932.
[5] K.D. Karlin, Y. Gultneh, Prog. Inorg. Chem. 35 (1987) 219.
[6] T.N. Sorrell, Tetrahedron 45 (1989) 3.
[7] K.D. Karlin, Z. Tyeklar, Adv. Inorg. Biochem. 9 (1994) 123.
[8] E.I. Solomon, M.D. Lowery, Science 259 (1993) 1575.
[9] L. Que, W.B. Tolman, Angew. Chem. Int. Ed. 41 (2002) 1114.
[10] P.L. Holland, W.B. Tolman, Coord. Chem. Rev. 192 (1999) 855.
[11] W. Kaim, J. Rall, Angew. Chem. Int. Ed. 35 (1996) 43.
[12] L.M. Mirica, X. Ottenwaelder, T.D.P. Stack, Chem. Rev. 104 (2004) 1013.
[13] T.D.P. Stack, Dalton Trans. (2003) 1881.
[14] J.A. Halfen, S. Mahapatra, E.C. Wilkinson, S. Kaderli, V.G. Young, L. Que, A.D. Zuberbühler, W.B. Tolman, Science 271 (1996) 1397.
[15] M.J. Henson, M.A. Vance, C.X. Zhang, H.C. Liang, K.D. Karlin, E.I. Solomon, J. Am. Chem. Soc. 125 (2003) 5186.
[16] J. Cahoy, P.L. Holland, W.B. Tolman, Inorg. Chem. 38 (1999) 2161.
[17] H.C. Liang, M.J. Henson, L.Q. Hatcher, M.A. Vance, C.X. Zhang, D. Lahti, S. Kaderli, R.D. Sommer, A.L. Rheingold, A.D. Zuberbuhler, E.I. Solomon, K.D. Karlin, Inorg. Chem. 43 (2004) 4115.
[18] V. Mahadevan, M.J. Henson, E.I. Solomon, T.D.P. Stack, J. Am. Chem. Soc. 122 (2000) 10249.
[19] T. Burmester, J. Comp. Physiol. B 172 (2002) 95.
[20] E.I. Solomon, M.J. Baldwin, M.D. Lowery, Chem. Rev. 92 (1992) 521.
[21] E.I. Solomon, U.M. Sundaram, T.E. Machonkin, Chem. Rev. 96 (1996) 2563.
[22] E.I. Solomon, F. Tuczek, D.E. Root, C.A. Brown, Chem. Rev. 94 (1994) 827.
[23] K.A. Magnus, H. Ton-That, J.E. Carpenter, Chem. Rev. 94 (1994) 727.
[24] R.H. Holm, P. Kennepohl, E.I. Solomon, Chem. Rev. 96 (1996) 2239.
[25] E.I. Solomon, K.W. Penfield, D.E. Wilcox, Struct. Bond. 53 (1983) 1.
[26] E.I. Solomon, Pure Appl. Chem. 55 (1983) 1069.
[27] K.E. Van Holde, K.I. Miller, H. Decker, J. Biol. Chem. 276 (2001) 15563.
[28] N.C. Eickman, R.S. Himmelwright, E.I. Solomon, Proc. Natl. Acad. Sci. U.S.A. 76 (1979) 2094.
[29] P. Gamez, I.A. Koval, J. Reedijk, Dalton Trans. (2004) 4079.
[30] M.E. Cuff, K.I. Miller, K.E. Van Holde, W.A. Hendrickson, J. Mol. Biol. 278 (1998) 855.
[31] B. Hazes, K.A. Magnus, C. Bonaventura, J. Bonaventura, Z. Dauter, K.H. Kalk, W.G.J. Hol, Protein Sci. 2 (1993) 597.
[32] K.A. Magnus, B. Hazes, H. Ton-That, C. Bonaventura, J. Bonaventura, W.G.J. Hol, Proteins Struct. Funct. Genet. 19 (1994) 302.
[33] D.M. Dooley, R.A. Scott, J. Ellinghaus, E.I. Solomon, H.B. Gray, Proc. Natl. Acad. Sci. U.S.A. 75 (1978) 3019.
[34] E.I. Solomon, D.M. Dooley, R.-H. Wang, H.B. Gray, M. Cerdonio, F. Mogno, G.L. Romani, J. Am. Chem. Soc. 98 (1976) 1029.
[35] T.H. Moss, D.C. Gould, A. Ehrenberg, J.S. Loehr, H.S. Mason, Biochemistry 12 (1973) 2444.
[36] N. Kitajima, Y. Moro-oka, Chem. Rev. 94 (1994) 737.
[37] E.I. Solomon, P. Chen, M. Metz, S.-K. Lee, A.E. Palmer, Angew. Chem. Int. Ed. 40 (2001) 4570.
[38] A.G. Blackman, W.B. Tolman, Struct. Bond. 97 (2000) 179.
[39] H. Decker, R. Dillinger, F. Tuczek, Angew. Chem. Int. Ed. 39 (2000) 1591.
[40] K. Lerch, Mol. Cell. Biochem. 52 (1983) 125.
[41] A.L. Hughes, Immunogenetics 49 (1999) 106.
[42] E. Jaenicke, H. Decker, ChemBioChem 5 (2004) 163.
[43] Y. Matoba, T. Kumagai, A. Yamamoto, H. Yoshitsu, M. Sugiyama, J. Biol. Chem. 281 (2006) 8981.
[44] E.J. Land, C.A. Ramsden, P.A. Riley, Acc. Chem. Res. 36 (2003) 300.
[45] B.J. Deverall, Nature 189 (1961) 311.
[46] Y. Xu, A.H. Stokes, R. Roskoski Jr., K.E. Vrana, J. Neurosci. Res. 54 (1998) 691.
[47] M. Asanuma, I. Miyazaki, N. Ogawa, Neurotox. Res. 5 (2003) 165.
[48] G.L. Woolery, L. Powers, M. Winkler, E.I. Solomon, K. Lerch, T.G. Spiro, Biochim. Biophys. Acta Protein Struct. Mol. Enzymol. 788 (1984) 155.
[49] N.C. Eickman, E.I. Solomon, J.A. Larrabee, T.G. Spiro, K. Lerch, J. Am. Chem. Soc. 100 (1978) 6529.
[50] R.S. Himmelwright, N.C. Eickman, C.D. LuBien, E.I. Solomon, J. Am. Chem. Soc. 102 (1980) 5378.
[51] A. Sanchez-Ferrer, J.N. Rodriguez-Lopez, F. Garcia-Canovas, F. Garcia-Carmona, Biochim. Biophys. Acta Protein Struct. Mol. Enzymol. 1247 (1995) 1.
[52] S. Mandal, D. Macikenas, J.D. Protasiewicz, L.M. Sayre, J. Org. Chem. 65 (2000) 4804.
[53] N. Kitajima, K. Fujisawa, C. Fujimoto, Y. Moro-oka, S. Hashimoto, T. Kitagawa, K. Toriumi, K. Tatsumi, A. Nakamura, J. Am. Chem. Soc. 114 (1992) 1277.
[54] P.K. Ross, E.I. Solomon, J. Am. Chem. Soc. 112 (1990) 5871.
[55] P.K. Ross, E.I. Solomon, J. Am. Chem. Soc. 113 (1991) 3246.
[56] M.J. Baldwin, D.E. Root, J.E. Pate, K. Fujisawa, N. Kitajima, E.I. Solomon, J. Am. Chem. Soc. 114 (1992) 10421.

[57] M. Tremolieres, J.G. Bieth, Phytochemistry 23 (1984) 501.
[58] A.M. Mayer, E. Harel, Phytochemistry 18 (1979) 193.
[59] T. Klabunde, C. Eicken, J.C. Sacchettini, B. Krebs, Nat. Struct. Biol. 5 (1998) 1084.
[60] H.H.T. Nguyen, A.K. Shiemke, S.J. Jacobs, B.J. Hales, M.E. Lidstrom, S.I. Chan, J. Biol. Chem. 269 (1994) 14995.
[61] H.-H.T. Nguyen, S.J. Elliott, J.H.-K. Yip, S.I. Chan, J. Biol. Chem. 273 (1998) 7957.
[62] R.L. Lieberman, D.B. Shrestha, P.E. Doan, B.M. Hoffman, T.L. Stemmler, A.C. Rosenzweig, Proc. Natl. Acad. Sci. U.S.A. 100 (2003) 3820.
[63] S.I. Chan, K.H.C. Chen, S.S.F. Yu, C.-L. Chen, S.S.J. Kuo, Biochemistry 43 (2004) 4421.
[64] R.L. Lieberman, A.C. Rosenzweig, Crit. Rev. Biochem. Mol. Biol. 39 (2004) 147.
[65] R.L. Lieberman, A.C. Rosenzweig, Nature 434 (2005) 177.
[66] R.S. Hanson, T.E. Hanson, Microbiol. Rev. 60 (1996) 439.
[67] J.P. Sullivan, D. Dickinson, H.A. Chase, Crit. Rev. Microbiol. 24 (1998) 335.
[68] R.A. Periana, G. Bhalla, W.J. Tenn, K.J.H. Young, X.Y. Liu, O. Mironov, C. Jones, V.R. Ziatdinov, J. Mol. Catal. A 220 (2004) 7.
[69] E. Pidcock, H.V. Obias, C.X. Zhang, K.D. Karlin, E.I. Solomon, J. Am. Chem. Soc. 120 (1998) 7841, and references therein.
[70] H.V. Obias, Y. Lin, N.N. Murthy, E. Pidcock, E.I. Solomon, M. Ralle, N.J. Blackburn, Y.-M. Neuhold, A.D. Zuberbuehler, K.D. Karlin, J. Am. Chem. Soc. 120 (1998) 12960.
[71] S. Mahapatra, J.A. Halfen, E.C. Wilkinson, G. Pan, X. Wang, V.G. Young, C.J. Cramer, L. Que, W.B. Tolman, J. Am. Chem. Soc. 118 (1996) 11555.
[72] S. Mahapatra, V.G. Young, S. Kaderli, A.D. Zuberbühler, W.B. Tolman, Angew. Chem. Int. Ed. 36 (1997) 130.
[73] S. Itoh, H. Nakao, L.M. Berreau, T. Kondo, M. Komatsu, S. Fukuzumi, J. Am. Chem. Soc. 120 (1998) 2890.
[74] S. Itoh, M. Taki, H. Nakao, P.L. Holland, W.B. Tolman, L. Que, S. Fukuzumi, Angew. Chem. Int. Ed. 39 (2000) 398.
[75] M. Taki, S. Itoh, S. Fukuzumi, J. Am. Chem. Soc. 123 (2001) 6203.
[76] K. Yoshizawa, Y. Shiota, J. Am. Chem. Soc. 128 (2006) 9873.
[77] E.A. Lewis, W.B. Tolman, Chem. Rev. 104 (2004) 1047.
[78] W.B. Tolman, Acc. Chem. Res. 30 (1997) 227.
[79] L.Q. Hatcher, K.D. Karlin, J. Biol. Inorg. Chem. 9 (2004) 669.
[80] S. Schindler, Eur. J. Inorg. Chem. (2000) 2311.
[81] G. Battaini, A. Granata, E. Monzani, M. Gullotti, L. Casella, Adv. Inorg. Chem. 58 (2006) 185.
[82] C.X. Zhang, H.-C. Liang, K.J. Humphreys, K.D. Karlin, Catal. Metal Complex. 26 (2003) 79.
[83] W.B. Tolman, J. Biol. Inorg. Chem. 11 (2006) 261.
[84] V. Mahadevan, R. Gebbink, T.D.P. Stack, Curr. Opin. Chem. Biol. 4 (2000) 228.
[85] S. Mahapatra, J.A. Halfen, E.C. Wilkinson, L. Que, W.B. Tolman, J. Am. Chem. Soc. 116 (1994) 9785.
[86] S. Mahapatra, J.A. Halfen, E.C. Wilkinson, G. Pan, C.J. Cramer, L. Que, W.B. Tolman, J. Am. Chem. Soc. 117 (1995) 8865.
[87] S. Mahapatra, J.A. Halfen, W.B. Tolman, J. Am. Chem. Soc. 118 (1996) 11575.
[88] A. Bérces, Inorg. Chem. 36 (1997) 4831.
[89] A. Bérces, Int. J. Quantum Chem. 65 (1997) 1077.
[90] C.J. Cramer, Y. Pak, Theor. Chem. Acc. 105 (2001) 477.
[91] C.J. Cramer, C.K. Kinsinger, Y. Pak, J. Mol. Struct. (Theochem) 632 (2003) 111.
[92] B.M.T. Lam, J.A. Halfen, V.G. Young Jr., J.R. Hagadorn, P.L. Holland, A. Lledos, L. Cucurull-Sanchez, J.J. Novoa, S. Alvarez, W.B. Tolman, Inorg. Chem. 39 (2000) 4059.
[93] J.L. Lewin, D.E. Heppner, C.J. Cramer, J. Biol. Inorg. Chem. 12 (2007) 1221.
[94] H. Koyama, T. Yoshino, Bull. Chem. Soc. Jpn. 45 (1972) 481.
[95] J.E. Richman, T.J. Atkins, J. Am. Chem. Soc. 96 (1974) 2268.
[96] P.E.M. Siegbahn, J. Biol. Inorg. Chem. 8 (2003) 577.
[97] N. Kitajima, T. Koda, S. Hashimoto, T. Kitagawa, Y. Moro-oka, J. Chem. Soc., Chem. Commun. (1988) 151.
[98] N. Kitajima, K. Fujisawa, Y. Morooka, K. Toriumi, J. Am. Chem. Soc. 111 (1989) 8975.
[99] P. Chen, E.I. Solomon, J. Inorg. Biochem. 88 (2002) 368.
[100] G. Aullon, S.M. Gorun, S. Alvarez, Inorg. Chem. 45 (2006) 3594.
[101] I. Sanyal, M. Mahroof-Tahir, M.S. Nasir, P. Ghosh, B.I. Cohen, Y. Gultneh, R.W. Cruse, A. Farooq, K.D. Karlin, S. Liu, J. Zubieta, Inorg. Chem. 31 (1992) 4322.
[102] H. Naka, Y. Kondo, S. Usui, Y. Hashimoto, M. Uchiyama, Adv. Synth. Catal. 349 (2007) 595.
[103] E. Pidcock, S. DeBeer, H.V. Obias, B. Hedman, K.O. Hodgson, K.D. Karlin, E.I. Solomon, J. Am. Chem. Soc. 121 (1999) 1870.
[104] H.-C. Liang, C.X. Zhang, M.J. Henson, R.D. Sommer, K.R. Hatwell, S. Kaderli, A.D. Zuberbühler, A.L. Rheingold, E.I. Solomon, K.D. Karlin, J. Am. Chem. Soc. 124 (2002) 4170.
[105] A. Company, L. Gomez, R. Mas-Balleste, I.V. Korendovych, X. Ribas, A. Poater, T. Parella, X. Fontrodona, J. Benet-Buchholz, M. Sola, L. Que, E.V. Rybak-Akimova, M. Costas, Inorg. Chem. 46 (2007) 4997.
[106] M. Costas, X. Ribas, A. Poater, J.M. LopezValbuena, R. Xifra, A. Company, M. Duran, M. Sola, A. Llobet, M. Corbella, M.A. Uson, J. Mahia, X. Solans, X. Shan, J. Benet-Buchholz, Inorg. Chem. 45 (2006) 3569.
[107] R. Menif, A.E. Martell, J. Chem. Soc., Chem. Commun. (1989) 1521.
[108] D. Utz, F.W. Heinemann, F. Hampel, D.T. Richens, S. Schindler, Inorg. Chem. 42 (2003) 1430.
[109] A. Company, D. Lamata, A. Poater, M. Sola, E.V. Rybak-Akimova, L. Que Jr., X. Fontrodona, T. Parella, A. Llobet, M. Costas, Inorg. Chem. 45 (2006) 5239.
[110] V. Mahadevan, Z. Hou, A.P. Cole, D.E. Root, T.K. Lal, E.I. Solomon, T.D.P. Stack, J. Am. Chem. Soc. 119 (1997) 11996.
[111] L.M. Mirica, D.J. Rudd, M.A. Vance, E.I. Solomon, K.O. Hodgson, B. Hedman, T.D.P. Stack, J. Am. Chem. Soc. 128 (2006) 2654.
[112] L.M. Mirica, M. Vance, D.J. Rudd, B. Hedman, K.O. Hodgson, E.I. Solomon, T.D.P. Stack, Science 308 (2005) 1890.
[113] X. Ottenwaelder, D.J. Rudd, M.C. Corbett, K.O. Hodgson, B. Hedman, T.D.P. Stack, J. Am. Chem. Soc. 128 (2006) 9268.
[114] D.J.E. Spencer, N.W. Aboelella, A.M. Reynolds, P.L. Holland, W.B. Tolman, J. Am. Chem. Soc. 124 (2002) 2108.
[115] D.J.E. Spencer, A.M. Reynolds, P.L. Holland, B.A. Jazdzewski, C. Duboc-Toia, L. Le Pape, S. Yokota, Y. Tachi, S. Itoh, W.B. Tolman, Inorg. Chem. 41 (2002) 6307.
[116] J.T. York, A. Llobet, C.J. Cramer, W.B. Tolman, J. Am. Chem. Soc. 129 (2007) 7990.
[117] N.W. Aboelella, B.F. Gherman, L.M.R. Hill, J.T. York, N. Holm, V.G. Young, C.J. Cramer, W.B. Tolman, J. Am. Chem. Soc. 128 (2006) 3445.
[118] P. Spuhler, M.C. Holthausen, Angew. Chem. Int. Ed. 42 (2003) 5961.
[119] H. Borzel, P. Comba, C. Katsichtis, W. Kiefer, A. Lienke, V. Nagel, H. Pritzkow, Chem. Eur. J. 5 (1999) 1716.
[120] H. Borzel, P. Comba, K.S. Hagen, C. Katsichtis, H. Pritzkow, Chem. Eur. J. 6 (2000) 914.
[121] P. Comba, A. Lienke, Inorg. Chem. 40 (2001) 5206.
[122] H. Borzel, P. Comba, K.S. Hagen, M. Kerscher, H. Pritzkow, M. Schatz, S. Schindler, O. Walter, Inorg. Chem. 41 (2002) 5440.
[123] K. Born, P. Comba, A. Daubinet, A. Fuchs, H. Wadepohl, J. Biol. Inorg. Chem. 12 (2007) 36.
[124] M.J. Begley, P. Hubberstey, C.E. Russell, P.H. Walton, J. Chem. Soc., Dalton Trans. (1994) 2483.
[125] O. Eisenstein, H. Getlicherman, C. Giessner-Prettre, J. Maddaluno, Inorg. Chem. 36 (1997) 3455.
[126] C.J. Cramer, Essentials of Computational Chemistry: Theories and Models, John Wiley & Sons, Chichester, 2004.
[127] R.J. Deeth, Struct. Bond. 113 (2004) 37.
[128] F. Maseras, K. Morokuma, J. Comp. Chem. 16 (1995) 1170.
[129] M. Dolg, U. Wedig, H. Stoll, H. Preuss, J. Chem. Phys. 86 (1987) 866.
[130] H. Stoll, B. Metz, M. Dolg, J. Comp. Chem. 23 (2002) 767.
[131] P.J. Hay, W.R. Wadt, J. Chem. Phys. 82 (1985) 299.
[132] P.J. Hay, W.R. Wadt, J. Chem. Phys. 82 (1985) 270.

[133] C.J. Cramer, D.G. Truhlar, Chem. Rev. 99 (1999) 2161.
[134] C.J. Cramer, B.A. Smith, W.B. Tolman, J. Am. Chem. Soc. 118 (1996) 11283.
[135] N.W. Aboelella, S. Kryatov, B.F. Gherman, W.W. Brennessel, V.G. Young, R. Sarangi, E. Rybak-Akimova, K.O. Hodgson, B. Hedman, E.I. Solomon, C.J. Cramer, W.B. Tolman, J. Am. Chem. Soc. 126 (2004) 16896.
[136] F. Tuczek, E.I. Solomon, J. Am. Chem. Soc. 116 (1994) 6916.
[137] Y. Takano, S. Kubo, T. Onisi, H. Isobe, Y. Yoshioka, K. Yamaguchi, Chem. Phys. Lett. 335 (2001) 395.
[138] M. Reiher, Faraday Dis. 135 (2007) 97.
[139] T. Ziegler, A. Rauk, E.J. Baerends, Theor. Chim. Acta 43 (1977) 261.
[140] L. Noodleman, J.G. Norman, J. Chem. Phys. 70 (1979) 4903.
[141] K. Yamaguchi, F. Jensen, A. Dorigo, K.N. Houk, Chem. Phys. Lett. 149 (1988) 537.
[142] L. Noodleman, D.A. Case, Adv. Inorg. Chem. 38 (1992) 423.
[143] L. Noodleman, C.Y. Peng, D.A. Case, J.-M. Mouesca, Coord. Chem. Rev. 144 (1995) 199.
[144] M.H. Lim, S.E. Worthington, F.J. Dulles, C.J. Cramer, in: B.B. Laird, R.B. Ross, T. Ziegler (Eds.), Chemical Applications of Density Functional Theory, American Chemical Society, Washington, DC, 1996, p. 402.
[145] W.T.G. Johnson, C.J. Cramer, Int. J. Quantum Chem. 85 (2001) 492.
[146] H. Isobe, Y. Takano, Y. Kitagawa, T. Kawakami, S. Yamanaka, K. Yamaguchi, K.N. Houk, Mol. Phys. 100 (2002) 717.
[147] C.R. Kinsinger, B.F. Gherman, L. Gagliardi, C.J. Cramer, J. Biol. Inorg. Chem. 10 (2005) 778.
[148] F. Neese, J. Phys. Chem. Solids 65 (2004) 781.
[149] G. Ghigo, M. Causa, A. Maranzana, G. Tonachini, J. Phys. Chem. A 110 (2006) 13270.
[150] R. Takeda, S. Yamanaka, K. Yamaguchi, Int. J. Quantum Chem. 106 (2006) 3303.
[151] B.H. Northrop, K.N. Houk, J. Org. Chem. 71 (2006) 3.
[152] L. Hindiyarti, P. Glarborg, P. Marshall, J. Phys. Chem. A 111 (2007) 3984.
[153] M. Jaworska, Chem. Phys. 332 (2007) 203.
[154] M. Shoji, K. Koizumi, Y. Kitagawa, S. Yamanaka, M. Okumura, K. Yamaguchi, Int. J. Quantum Chem. 107 (2007) 609.
[155] B.V. Popp, J.E. Wendlandt, C.R. Landis, S.S. Stahl, Angew. Chem. Int. Ed. 46 (2007) 601.
[156] A.H. Winter, D.E. Falvey, C.J. Cramer, B.F. Gherman, J. Am. Chem. Soc. 129 (2007) 10113.
[157] C.J. Cramer, M. Wloch, P. Piecuch, C. Puzzarini, L. Gagliardi, J. Phys. Chem. A 110 (2006) 1991.
[158] C.J. Cramer, A. Kinal, M. Wloch, P. Piecuch, L. Gagliardi, J. Phys. Chem. A 110 (2006) 11557.
[159] Y.H. Shao, M. Head-Gordon, A.I. Krylov, J. Chem. Phys. 118 (2003) 4807.
[160] A. de la Lande, V. Moliner, O. Parisel, J. Chem. Phys. 126 (2007).
[161] E.R. Davidson, A.E. Clark, Phys. Chem. Chem. Phys. 9 (2007) 1881.
[162] F. Neese, J. Biol. Inorg. Chem. 11 (2006) 702.
[163] M.W. Schmidt, M.S. Gordon, Annu. Rev. Phys. Chem. 49 (1998) 233.
[164] B.O. Roos, P.R. Taylor, P.E.M. Siegbahn, Chem. Phys. 48 (1980) 157.
[165] K. Andersson, P.-Å. Malmqvist, B.O. Roos, A.J. Sadlej, K. Wolinski, J. Phys. Chem. 94 (1990) 5483.
[166] K. Andersson, P.-Å. Malmqvist, B.O. Roos, J. Chem. Phys. 96 (1992) 1218.
[167] P. Piecuch, K. Kowalski, I.S.O. Pimienta, P.-D. Fan, M. Lodriguito, M.J. McGuire, S.A. Kucharski, T. Kuś, M. Musiał, Theor. Chem. Acc. 112 (2004) 349.
[168] A. Kinal, P. Piecuch, J. Phys. Chem. A 110 (2006) 367.
[169] A. Kinal, P. Piecuch, J. Phys. Chem. A 111 (2007) 734.
[170] X.-Y. Liu, A.A. Palacios, J.J. Novoa, S. Alvarez, Inorg. Chem. 37 (1998) 1202.
[171] M.J. Henson, P. Mukherjee, D.E. Root, T.D.P. Stack, E.I. Solomon, J. Am. Chem. Soc. 121 (1999) 10332.
[172] A.D. Becke, Phys. Rev. A 38 (1988) 3098.
[173] C. Lee, W. Yang, R.G. Parr, Phys. Rev. B 37 (1988) 785.
[174] A.D. Becke, J. Chem. Phys. 98 (1993) 5648.
[175] P.J. Stephens, F.J. Devlin, C.F. Chabalowski, M.J. Frisch, J. Phys. Chem. 98 (1994) 11623.
[176] W.J. Hehre, L. Radom, P.V.R. Schleyer, J.A. Pople, Ab Initio Molecular Orbital Theory, Wiley, New York, 1986.
[177] G.S. Nikolov, H. Mikosch, G. Bauer, J. Mol. Struct. (Theochem.) 499 (2000) 35.
[178] K. Kowalski, P. Piecuch, J. Chem. Phys. 113 (2000) 18.
[179] P. Piecuch, K. Kowalski, in: J. Leszczyński (Ed.), Computational Chemistry: Reviews of Current Trends, World Scientific, Singapore, 2000, p. 1.
[180] P. Piecuch, K. Kowalski, I.S.O. Pimienta, M.J. McGuire, Int. Rev. Phys. Chem. 21 (2002) 527.
[181] M. Włoch, M. Lodriguito, P. Piecuch, J.R. Gour, Mol. Phys. 104 (2006) 2149.
[182] P. Piecuch, M. Włoch, J. Chem. Phys. 123 (2005) 224105.
[183] P. Piecuch, M. Włoch, J.R. Gour, A. Kinal, Chem. Phys. Lett. 418 (2005) 463.
[184] I. Özkan, A. Kinal, M. Balci, J. Phys. Chem. A 108 (2004) 507.
[185] M.J. McGuire, P. Piecuch, J. Am. Chem. Soc. 127 (2005) 2608.
[186] C. Adamo, V. Barone, J. Chem. Phys. 108 (1998) 664.
[187] J. Tao, J.P. Perdew, V.N. Staroverov, G.E. Scuseria, Phys. Rev. Lett. 91 (2003) 146401.
[188] M.F. Rode, H.-J. Werner, Theor. Chem. Acc. 114 (2005) 309.
[189] C. Herrmann, L. Yu, M. Reiher, J. Comp. Chem. 27 (2006) 1223.
[190] P.E.M. Siegbahn, J. Comp. Chem. 22 (2001) 1634.
[191] P.E.M. Siegbahn, M. Wirstam, J. Am. Chem. Soc. 123 (2001) 11819.
[192] J.P. Piquemal, J. Maddaluno, B. Silvi, C. Giessner-Prettre, New J. Chem. 27 (2003) 909.
[193] J.P. Piquemal, J. Pilme, J. Mol. Struct. (Theochem.) 764 (2006) 77.
[194] S. Alvarez, A.A. Palacios, G. Aullon, Coord. Chem. Rev. 186 (1999) 431.
[195] M. Metz, E.I. Solomon, J. Am. Chem. Soc. 123 (2001) 4938.
[196] F. Bernardi, A. Bottoni, R. Casadio, P. Fariselli, A. Rigo, Inorg. Chem. 35 (1996) 5207.
[197] A. Bérces, Chem. Eur. J. 4 (1998) 1297.
[198] J. Maddaluno, C. Geissner-Prettre, Inorg. Chem. 30 (1991) 3439.
[199] R.R. Jacobson, Z. Tyeklar, A. Farooq, K.D. Karlin, S. Liu, J. Zubieta, J. Am. Chem. Soc. 110 (1988) 3690.
[200] F. Bernardi, A. Bottoni, R. Casadio, P. Fariselli, A. Rigo, Int. J. Quantum Chem. 58 (1996) 109.
[201] M. Flock, K. Pierloot, J. Phys. Chem. A 103 (1999) 95.
[202] U. Schollwöck, Rev. Mod. Phys. 77 (2005) 259.
[203] K.H. Marti, I.M. Ondík, G. Moritz, M. Reiher, J. Chem. Phys., in press.
[204] R.G. Parr, L.v. Szentpaly, S. Liu, J. Am. Chem. Soc. 121 (1999) 1922.
[205] S. Fox, K.D. Karlin, in: J.S. Valentine, C.S. Foote, A. Greenberg, J.F. Liebman (Eds.), Active Oxygen in Biochemistry, Blackie Academic & Professional/Chapman & Hall, Glasgow, Scotland, 1995, p. 188.
[206] L.Q. Hatcher, K.D. Karlin, Adv. Inorg. Chem. 58 (2006) 131.
[207] S. Itoh, Y. Tachi, Dalton Trans. (2006) 4531.
[208] J. Shearer, C.X. Zhang, L.N. Zakharov, A.L. Rheingold, K.D. Karlin, J. Am. Chem. Soc. 127 (2005) 5469.
[209] P.E.M. Siegbahn, J. Biol. Inorg. Chem. 8 (2003) 567.
[210] T. Lind, P.E.M. Siegbahn, R.H. Crabtree, J. Phys. Chem. B 103 (1999) 1193.
[211] J.N. Rodriguez-Lopez, J. Tudela, R. Varon, F. Garcia-Carmona, F. Garcia-Canovas, J. Biol. Chem. 267 (1992) 3801.
[212] P.E.M. Siegbahn, J. Biol. Inorg. Chem. 11 (2006) 695.
[213] C.R. Kinsinger, Ph.D. Thesis, University of Minnesota, Minneapolis, MN, 2004.
[214] T. Vreven, K. Morokuma, Ö. Farkas, H.B. Schlegel, M.J. Frisch, J. Comp. Chem. 24 (2003) 760.
[215] A.K. Rappé, C.J. Casewit, K.S. Colwell, W.A. Goddard, W.M. Skiff, J. Am. Chem. Soc. 114 (1992), 10024; 10035; 10046.
[216] B.J. Lynch, P.L. Fast, M. Harris, D.G. Truhlar, J. Phys. Chem. A 104 (2000) 4811.
[217] P.P.Y. Chen, S.I. Chan, J. Inorg. Biochem. 100 (2006) 801.
[218] B.F. Gherman, W.B. Tolman, C.J. Cramer, J. Comp. Chem. 27 (2006) 1950.

[219] P.E.M. Siegbahn, J. Biol. Inorg. Chem. 9 (2004) 577.
[220] J.M. Mayer, Acc. Chem. Res. 31 (1998) 441.
[221] C. Glaser, Chem. Ber. 2 (1869) 422.
[222] L. Fomina, B. Vazquez, E. Tkatchouk, S. Fomine, Tetrahedron 58 (2002) 6741.
[223] M. Taki, S. Itoh, S. Fukuzumi, J. Am. Chem. Soc. 124 (2002) 998.
[224] E. Tkatchouk, L. Fomina, E. Rivera, S. Fomine, J. Mol. Struct. (Theochem.) 729 (2005) 147.
[225] L.-S. Wang, H. Wu, S.R. Desai, L. Lou, Phys. Rev. B 53 (1996) 8028.
[226] P.L. Holland, C.J. Cramer, E.C. Wilkinson, S. Mahapatra, K.R. Rodgers, S. Itoh, M. Taki, S. Fukuzumi, L. Que, W.B. Tolman, J. Am. Chem. Soc. 122 (2000) 792.
[227] R.J.H. Clark, T.J. Dines, Angew. Chem. Int. Ed. 25 (1986).
[228] D.P. Strommen, J. Chem. Ed. 69 (1992) 803.
[229] B.B. Johnson, W.L. Peticolas, Annu. Rev. Phys. Chem. 27 (1976) 465.
[230] M.J. Baldwin, P.K. Ross, J.E. Pate, Z. Tyeklár, K.D. Karlin, E.I. Solomon, J. Am. Chem. Soc. 113 (1991) 8671.
[231] N.W. Aboelella, J.T. York, A.M. Reynolds, K. Fujita, C.R. Kinsinger, C.J. Cramer, C.G. Riordan, W.B. Tolman, Chem. Commun. (2004) 1716.
[232] C.J. Cramer, W.B. Tolman, K.H. Theopold, A.L. Rheingold, Proc. Natl. Acad. Sci. U.S.A. 100 (2003) 3635.
[233] P. Chen, D.E. Root, C. Campochiaro, K. Fujisawa, E.I. Solomon, J. Am. Chem. Soc. 125 (2003) 466.
[234] C.J. Cramer, W.B. Tolman, Acc. Chem. Res. 40 (2007) 601.
[235] R.S. Himmelwright, N.C. Eickman, C.D. LuBien, E.I. Solomon, K. Lerch, J. Am. Chem. Soc. 102 (1980) 7339.
[236] C. Eicken, F. Zippel, K. Buldt-Karentzopoulos, B. Krebs, FEBS Lett. 436 (1998) 293.
[237] E. Pidcock, H.V. Obias, M. Abe, H.-C. Liang, K.D. Karlin, E.I. Solomon, J. Am. Chem. Soc. 121 (1999) 1299.
[238] G.L. Estiú, M.C. Zerner, J. Am. Chem. Soc. 121 (1999) 1893.
[239] J.C. Slater, Adv. Quantum Chem. 6 (1972) 1.
[240] K.H. Johnson, Adv. Quantum Chem. 7 (1973) 143.
[241] D.A. Case, Annu. Rev. Phys. Chem. 33 (1982) 151.
[242] K.H. Johnson, Annu. Rev. Phys. Chem. 26 (1975) 39.
[243] L. Noodleman, J. Chem. Phys. 74 (1981) 5737.
[244] P.K. Ross, M.D. Allendorf, E.I. Solomon, J. Am. Chem. Soc. 111 (1989) 4009.
[245] S. Hirata, M. Head-Gordon, Chem. Phys. Lett. 302 (1999) 375.
[246] J.E. Ridley, M.C. Zerner, Theor. Chim. Acta 32 (1973) 111.
[247] J.E. Ridley, M.C. Zerner, Theor. Chim. Acta 42 (1976) 223.
[248] M.C. Zerner, G.H. Loew, R.F. Kirchner, U.T. Mueller-Westerhoff, J. Am. Chem. Soc. 102 (1980) 589.
[249] J.L. DuBois, P. Mukherjee, A.M. Collier, J.M. Mayer, E.I. Solomon, B. Hedman, T.D.P. Stack, K.O. Hodgson, J. Am. Chem. Soc. 119 (1997) 8578.
[250] V. Mahadevan, J.L. DuBois, B. Hedman, K.O. Hodgson, T.D.P. Stack, J. Am. Chem. Soc. 121 (1999) 5583.
[251] A. van der Avoird, P. Ros, Theor. Chim. Acta 4 (1966) 13.